Journal of Aerosol Science 155 (2021) 105746

Contents lists available at ScienceDirect

Journal of Aerosol Science

journal homepage: http://www.elsevier.com/locate/jaerosci

Tutorial: Langevin Dynamics methods for aerosol particle trajectory simulations and collision rate constant modeling

Vikram Suresh, Ranganathan Gopalakrishnan *

Department of Mechanical Engineering, The University of Memphis, Memphis, TN, USA

ARTICLE INFO

Keywords:
Langevin dynamics
Collision rate constant
Trajectory simulations
Single particle mass transfer
Transition regime processes
Diffusional transport kinetics

ABSTRACT

The Langevin Dynamics (LD) method (also known in the literature as Brownian Dynamics) is routinely used to simulate aerosol particle trajectories for transport rate constant calculations as well as to understand aerosol particle transport in internal and external fluid flows. This tutorial intends to explain the methodological details of setting up a LD simulation of a population of aerosol particles and to deduce rate constants from an ensemble of classical trajectories. We discuss the applicability and limitations of the translational Langevin equation to model the combined stochastic and deterministic motion of particles in fields of force or fluid flow. The drag force and stochastic "diffusion" force terms that appear in the Langevin equation are discussed elaborately, along with a summary of common forces relevant to aerosol systems (electrostatic, gravity, van der Waals, …); a commonly used first order and a fourth order Runge-Kutta time stepping schemes for linear stochastic ordinary differential equations are presented. A MATLAB® implementation of a LD computer code for simulating particle settling under gravity using the first order scheme is included for illustration. Scaling analysis of aerosol transport processes and the selection of timestep and domain size for trajectory simulations are demonstrated through two specific aerosol processes: particle diffusion charging and coagulation. Fortran® implementations of the first order and fourth order time-stepping schemes are included for simulating the 3D motion of a particle in a periodic domain. Potential applications and caveats to the usage of LD are included as a summary.

1. Introduction

The calculation of particle trajectories in the context of classical physics that permits the knowledge of both position and velocity with complete certainty by integrating Newton's Second law of motion, (i. e.) position $\vec{r}_p(t)$ and velocity $\vec{v}_p(t)$ timeseries, is of fundamental interest for visualizing aerosol particle dynamics, developing models of collision/reaction rate constants for single particle-level mass transfer processes as well as to predict the transport of populations of aerosol particles and can be accomplished at a relatively modest computational cost by integrating Langevin-type ordinary differential equations (ODEs) of motion. The term *particle* is broadly used here to denote nm – μm sized solid/liquid aerosol particles (spherical or arbitrary shaped), nm-sized macromolecules or molecular ions suspended in a flowing/stagnant background gas in the presence/absence of external electric/magnetic fields. In this tutorial article, we focus on the methodological details of solving the Langevin equation of motion to calculate particle trajectories and discuss two examples on the use of an ensemble of computed trajectories to infer single particle mass transfer rate constants. The

* Corresponding author.
E-mail address: rgplkrsh@memphis.edu (R. Gopalakrishnan).

https://doi.org/10.1016/j.jaerosci.2021.105746
Received 10 December 2020; Received in revised form 5 January 2021; Accepted 5 January 2021
Available online 7 February 2021
0021-8502/

Nomenclature (in order of appearance)

$\vec{r}_p(t)$	Particle position
$\vec{v}_p(t)$	Particle velocity
Re_p	Flow Reynolds number based on particle size
Ma_p	Flow Mach number based on particle velocity
$\vec{F}_D$	Drag force exerted by the gas medium on a particle
T_g	Gas temperature
p_g	Gas pressure
$\vec{F}_B(t)$	Time-dependent stochastic force experienced by the particle
t_r	Particle relaxation or thermal equilibration timescale
t_s	Particle transport timescale
$\vec{F}_{ext}$	Externally applied force on a particle
λ_{mpp}	Particle's mean persistence path
l_{sys}	System length scale
m_p	Particle mass
f_p	Particle friction factor
n_p	Particle number concentration
D_p	Particle mass diffusion constant
ζ_p	Particle electrical mobility
z_p	Particle electric charge
e	Magnitude of charge on an electron
k_B	Boltzmann constant
Kn_D	Diffusive Knudsen number for single particle mass transfer
Kn	Momentum Knudsen number for single particle momentum transfer
λ_g	Gas mean free path
l_p	Particle size descriptor
a_p	Radius of a spherical particle
PA	Orientation-averaged projected area of an arbitrary shaped particle
R_h	Capacitance or hydrodynamic radius of an arbitrary shaped particle
$\overline{\overline{f}}_p^T$	Single particle friction tensor
f_p^T	Single particle scalar friction factor
μ_g	Gas viscosity
ξ	Momentum accommodation coefficient
Ω_p	Particle momentum transfer collision cross-section
$\alpha_1, \alpha_2, \alpha_3$	Gas-specific coefficients in the calculation of f_p
η_v	Particle volume fraction
$\vec{v}_g$	Gas (continuum) velocity field
$\vec{F}_i$	Hydrodynamic force on the i^{th} sphere
$\overline{\overline{V}}_{ij}$	Perturbation tensor
f_i	Scalar friction factor of the i^{th} sphere
$\vec{r}_{ij}$	Position of sphere j relative to sphere i
r_{ij}	Distance between spheres i and j
$q_2^{(i)}(r_{ij}), q_3^{(i)}(r_{ij})$	Functions that appear in $\overline{\overline{V}}_{ij}$
$A_{3N\times 3N}$	Coefficient matrix of size $3N \times 3N$
$X_{3N\times 1}$	Solution vector of size $3N \times 1$
$B_{3N\times 1}$	Column vector of size $3N \times 1$
$\delta(\cdot)$	Delta function
γ_{ij}	Coefficient that appears in the variance of $\vec{F}_B$
$\Phi(r)$	Particle-particle interaction potential
$z_{1,2}$	Elementary charges of particles (1, 2)
ε_0	Permittivity of vacuum
ε_r	Particle dielectric constant
r	Radial separation between particles (1, 2)
$R_{1,2}$	Radius of particles (1, 2)

A	Particle Hamaker constant
m_1	Mass of particle 1
$\vec{E}(\vec{r}_1(t),t)$	Spatially and/or temporally varying electric field
$\vec{B}(\vec{r}_1(t),t)$	Spatially and/or temporally varying magnetic field
$\vec{v}_g(\vec{r}_1(t),t)$	Local fluid velocity
$\vec{F}_1$	Force on particle 1
λ_D	Debye length
n_i	Ion concentration
$\vec{g}$	Acceleration due to gravity
N	Number of particles
t_{ext}	Timescale of variation of $\vec{F}_{ext}$
$\vec{R}_r$	Normally distributed random position vector
$\vec{R}_v$	Normally distributed random velocity vector
Δt	Simulation timestep with units
$\boldsymbol{X}$	Solution vector
$\dot{\boldsymbol{X}}$	Time derivative of solution vector
$\boldsymbol{F}(\boldsymbol{X},t)$	Deterministic vector
$\boldsymbol{\Pi}(t)$	Stochastic vector
$\boldsymbol{D},\boldsymbol{c}_j,\boldsymbol{a}_{ji},\boldsymbol{\alpha}_i,\boldsymbol{q}_j$	Coefficients that appear in Eq. 17
ρ_p	Particle density
H	Height from which particle is released
z	Vertical coordinate
t_S	Average particle settling time
σ_S	Standard deviation of particle settling time
N_T	Number of trials
μ,k,σ	Parameters of generalized extreme value distribution
R_{pi}	Particle-ion collision rate
z_i	Ion charge
β_{pi}	Particle-ion collision kernel or collision rate constant
Φ_{pi}	Particle-ion interaction potential
L	Side of cubic periodic domain with units
τ	Average particle-ion collision time with units
m_i	Ion mass
f_i	Ion scalar friction factor
$\vec{r}_i^*$	Non-dimensional ion position
$\vec{v}_i^*$	Non-dimensional ion velocity
t^*	Non-dimensional time
Δt^*	Non-dimensional timestep
Ψ_E	Particle-ion electrostatic potential energy ratio
$\eta_c(\Psi_E),\eta_f(\Psi_E)$	Continuum and free molecular enhancement factors
H	Non-dimensional collision kernel
L^*	Non-dimensional side of cubic periodic domain
T^*	Non-dimensional timestep factor
EB method	First order accurate time stepping scheme given by eq. 14
RK method	Fourth order accurate time stepping scheme given by eq. 17
μ	Location parameter that appears in eq. 29
H_{RK}	H calculated using LD implemented using the RK method
H_{EB}	H calculated using LD implemented using the EB method
$H_{Eq.29}$	H calculated using eq. 29
ϑ_i	Volume of particle i
m_{ij}	Reduced mass
f_{ij}	Reduced friction factor
a_{ij}	Sum of particle radii
β_{ij}	Particle-particle coagulation kernel or coagulation rate constant
τ^*	Dimensionless average particle-particle collision time
τ_k	Dimensionless particle-particle collision time in trial k
R_{ij}	Collision rate of particle i and particle j

$H_{Eq.33}$	H calculated using eq. 33
H_N	H calculated using LD by simulating N particles in a periodic domain
$\left\|\delta\vec{F}_D^{\,*}\right\|^{max}$	Maximum of hydrodynamic force perturbation terms $\delta\vec{F}_{D,i}$
$\delta\vec{F}_{D,i}$	Hydrodynamic force perturbation terms
$\left\|\vec{r}_{ij}^{\,*}\right\|^{min}$	Minimum of particle pairwise seperations for all pairs $1 \le i \le N, 1 \le j \ne i \le N$
β_r	Ratio of collision kernel calculated using LD and using eq. 33

interested reader is referred to the pioneering work of Uhlenbeck and Ornstein (1930) that presents an analysis of the mean values of the velocity and mean squared displacement of a free particles subject to stochastic forces from a fluid medium and establishes the connection of the Langevin equation to the Fokker-Planck partial differential equations for the phase-space (velocity and position) distribution functions (Risken & Frank, 1996). Further, in a seminal review, Chandrasekhar (1943) presents a detailed overview of the Langevin equation, the underlying probabilistic aspects and applications to colloidal and astrophysical problems. The widespread use of Langevin equations to model driven-dissipative systems is evident from its usage in diverse fields such as physics, engineering, finance and several textbooks on this topic (Coffey et al., 2004; Risken & Frank, 1996; Schuss, 2013). We restrict our scope to walking the interested reader through the steps of setting up equations of motion to calculate particle trajectories under the influence of deterministic and stochastic forces and excuse ourselves from elaborate discussions of the modeling of the physical processes themselves. Specifically, the reader is referred to prior research articles on particle charging modeling (Chahl & Gopalakrishnan, 2019; Gopalakrishnan et al., 2013a, 2013b; Gopalakrishnan & Hogan, 2012; Li et al., 2020; Li & Gopalakrishnan, 2021; Ouyang et al., 2012) and particle coagulation modeling (Gopalakrishnan et al., 2011; Gopalakrishnan & Hogan, 2011; Thajudeen et al., 2012) using Langevin Dynamics. The tutorial is organized as follows: the *Methods* section discusses the Langevin ODE for particle translational motion; various particle-gas, particle-particle, particle-flow and particle-field interactions relevant to aerosol systems; two numerical schemes for integrating the Langevin ODE. Subsequently, in the *Demonstrations* section, we discuss two case studies of using LD to model the collision rate constant for aerosol particle diffusion charging and coagulation. We conclude with a *Summary* of the LD methodology, potential applications and caveats to the usage of LD for modeling particle trajectories in gas-phase systems such as aerosols and dusty plasmas.

2. Methods

2.1. Langevin equation of motion

The Langevin Dynamics (LD) methodology consists of essentially applying Newton's II law to model the motion of a suspended particle that is much heavier than the molecules of the background gas (Mazur & Oppenheim, 1970), while including the systematic resistance to particle motion exerted by the gas medium (in the $Re_p \to 0,\ Ma_p \to 0$ limit) as a time-averaged continuum drag force $\vec{F}_D$ and the random thermal impulses exerted by the gas molecules on a particle through discrete impacts, that physically manifest as Brownian motion at a given gas temperature T_g, as a time-dependent stochastic force $\vec{F}_B(t)$ (Chandrasekhar, 1943). LD assumes that the particle is in thermal equilibrium with the background gas through sufficiently many particle-gas molecule collisions: in other words, LD-calculated trajectories represent average behavior in the limit of sufficiently long observation times over which a particle undergoes these collisions. Thus, for high or atmospheric pressure systems, LD is an efficient formulation to represent particle stochastic and deterministic motion due to rapid relaxation of particles with the background gas: $t_r \ll t_s$, where t_r is the timescale over which the particle velocity relaxes to an equilibrium Maxwell-Boltzmann distribution through collisions with the gas molecules and t_s is the timescale of interest for particle transport. For low pressure systems, LD provides increasingly accurate results in the limit of $t_s \gg t_r$ and is appropriate generally, *except* when one is interested in particle transport timescales that are comparable or shorter than the relaxation times (i. e.) $t_s \tilde{} < t_r$. In such cases, a LD description may be abandoned in favor of a *direct* numerical simulation of the particles and the molecules constituting the background gas using molecular dynamics (MD) simulation methods (see for examples (Bird, 1994; Collins et al., 1996; Daneshian & Assadi, 2014; Goudeli & Pratsinis, 2016; Hawa & Zachariah, 2007; Koparde & Cummings, 2008; Mazzone, 2000; Naicker et al., 2005; Ogawa, 2005; Yi et al., 2005; Zhu, 1996),), that is considerably more computationally expensive than LD, or a Monte-Carlo (MC) type approach (see for examples (Bardsley & Wadehara, 1980; Kruis et al., 2000; Lin & Bardsley, 1977; Morán, Yon, & Poux, 2020; Morán, Yon, Poux, et al., 2020; Nowakowski & Sitarski, 1981; Rosner et al., 2003; Tandon & Rosner, 1999; Zahaf et al., 2015),) of accounting for particle-gas molecule collisions *probabilistically*. Lazzari et al. (2016) present a detailed summary of various computational methods that may be employed to unravel aggregation phenomena in diverse particulate systems considering the interplay of particle-particle interactions and solvent effects.

LD captures the particle-gas hydrodynamic interactions $(\vec{F}_D, \vec{F}_B)$ *implicitly* without needing to account for the details of individual particle-gas molecule collisions (Deutch & Oppenheim, 1971) while allowing the inclusion of all other external forces $\vec{F}_{ext}$ that act on the particle *explicitly* (Kim & Oppenheim, 1972), thus allowing the description of a particle's motion in the presence of a background gas by solving exactly *one* stochastic ODE of the form (Albers et al., 1971; Masters & Madden, 1981a):

$$m_p \frac{d\vec{v}_p}{dt} = \vec{F}_D + \vec{F}_B + \vec{F}_{ext} \tag{1}$$

The transport regime of particle motion in the presence of neutral gas molecules is typically established by comparing the particle's mean persistence path $\lambda_{mpp} \equiv \frac{\sqrt{m_p k_B T_g}}{f_p}$ at a specific gas temperature $k_B T_g$ and pressure p_g with a suitable system length scale l_{sys} to derive a diffusive Knudsen number $Kn_D \equiv \frac{\lambda_{mpp}}{l_{sys}}$ of particle mass transfer valid for dilute systems in which $\lambda_{mpp} \ll n_p^{-\frac{1}{3}}$ (Dawes & Sceats, 1988; Gopalakrishnan & Hogan, 2011; Thajudeen et al., 2012; Chahl & Gopalakrishnan, 2019); here m_p is the particle mass, f_p is the particle scalar friction factor, related to the particle mass diffusivity D_p via the Stokes-Einstein relationship $D_p = \frac{k_B T_g}{f_p}$ and to the particle electrical mobility $\zeta_p = \frac{z_p e}{f_p}$ and elementary particle charge z_p, $n_p^{-\frac{1}{3}}$ is the nominal particle-particle spacing based on the particle number concentration n_p. While the definition of Kn_D may be generalized based on $n_p^{-\frac{1}{3}}$ (Morán et al., 2020a, 2020b) for concentrated mass transfer regimes, for simplicity, we discuss dilute interactions between particles here. By definition, $Kn_D \to 0$ denotes the diffusive or continuum trajectories of particles and $Kn_D \to \infty$ represents the free molecular or ballistic motion of particles. λ_{mpp} must be distinguished from the more commonly used gas mean free path λ_g – the former may be interpreted as the average distance travelled by the *particle* before it changes direction completely due to diffusional collisions with gas molecules that alter its trajectory through space. The latter is a statistical quantity with a precise definition as the average distance travelled by *gas molecules* (not the particle) between collisions with other molecules. λ_{mpp} is typically used to characterize the nature of particle motion in the context of *mass transfer* of a particle onto another particle (charging, coagulation, condensation, …) or a surface (deposition, filtration, sedimentation, precipitation, impaction, bounce, resuspension, …). The regime of *momentum transfer* on to or from a particle to the gas is established by comparing λ_g to a suitable particle size descriptor l_p to derive the momentum Knudsen number $Kn \equiv \frac{\lambda_g}{l_p}$, with $Kn \to 0$ representing the continuum regime of fluid flow and $Kn \to \infty$ corresponding to the free molecular regime. The particle radius a_p is the obvious choice for spherical shapes whereas the use of $l_p = \frac{PA}{\pi R_h}$ has been shown to be valid for particles of arbitrary shape (Dahneke, 1973a, 1973b, 1973c; Zhang et al., 2012; Gopalakrishnan et al., 2015b; Thajudeen, Jeon, & Hogan, 2015); here, PA is the orientation-averaged projected area and R_h is the capacitance of the particle shape (elaborated upon in Section 2.2). It is noted that Kn_D and Kn, similar to pressure p_g and temperature T_g being independent thermodynamic properties of a gas, can represent different regimes of particle mass and momentum transfer, respectively (Thajudeen et al., 2012). It is conceivable that a particle may simultaneously considered to be undergoing mass transfer in the continuum regime while the gas medium exerts a transition regime drag (momentum transfer), or any combinations thereof, by virtue of $0 < Kn_D < \infty, 0 < Kn < \infty$ independently, for a population of particles. For example, the diffusional deposition of particles from a gas flow at low pressure through a tube is an instance in which Kn_D is small owing to $l_{sys} \gg \lambda_{mpp}$ for mass transfer while single particle momentum transfer takes place at high Kn as $l_p \ll \lambda_g$. For the same set of conditions, if one considered particle-particle coagulation, driven by diffusion, Kn_D would be high, as, in this case, $l_{sys} = l_p \ll \lambda_{mpp}$ for single particle mass transfer.

Time resolved solutions to eq. (1) allow the quantification of the effects of both deterministic and stochastic forces on a particle's trajectory through space and time, acting as a bridge computational technique between field theories used to describe the continuum/diffusive limit of particle motion ($Kn_D \to 0, p_g \to \infty$), wherein the particle inertia is negligible $\left(m_p \frac{d\vec{v}_p}{dt} \ll \vec{F}_B \right)$ compared to thermalizing stochastic forces allowing the assumption of instant equilibration, and kinetic theories valid in the low pressure free molecular/ballistic limit ($Kn_D \to \infty, p_g \to 0$) wherein the fluid drag exerted by the gas on the particle vanishes ($\vec{F}_D \to 0$) along with the absence of random collisions with gas molecules ($\vec{F}_B \to 0$). LD simulations allow the computationally inexpensive description of particle motion in the finite Kn_D, p_g *transition regime* wherein the trajectories are influenced by both non-negligible inertia, short timescale thermal impulses as well as long timescale drag forces exerted by the gas medium. LD is thus a niche transition regime computational method that allows the exploration of the interplay of dissipative particle-gas interactions (drag), stochastic particle-gas interactions (Brownian motion) and deterministic or potential interactions between particles, force fields and fluid flows. In Sections 2.2–2.4, we discuss the functional forms of $\vec{F}_D, \vec{F}_B, \vec{F}_{ext}$ to be used in eq. (1) for modeling particle motion. The coupled translation and rotation of aerosol particles may also be modeled with an additional equation for the conservation of angular momentum along with expressions for the resistance torques, stochastic torques and deterministic torques, analogous to forces in the case of translation. We consider these aspects, although important, to be beyond our scope and refer the interested reader to the literature on rotational Brownian motion (Hubbard, 1972, 1973, 1977; Masters & Madden, 1981b); the coupling between translation and rotation (Brenner, 1965, 1967); calculation of resistance tensors for rotational motion in the continuum regime (Brenner, 1963, 1964) and transition regime (Corson et al., 2017b, 2018a); and numerical methods for integrating coupled translation and rotational Langevin equations (Davidchack et al., 2009, 2017; Delong et al., 2015; Gordon et al., 2009; Ilie et al., 2015; Sun et al., 2008; Wu & Brooks, 2011).

2.2. Hydrodynamic drag force $\vec{F}_D$ in dilute particle concentration regimes

For instances wherein particle rotation minimally influences their transport and may be conveniently ignored and the orientation assumed to be frozen in time, particles trajectories can be calculated by considering translation only. For an *isolated*, arbitrary shaped particle slowly moving through an unbounded fluid in the $Re_p \to 0, Ma_p \to 0$ limit, the hydrodynamic drag $\vec{F}_D$ exerted by the gas

medium is calculated as the dot product of a single particle friction tensor $\overset{=T}{f}_p$ and particle velocity $\vec{v}_p$ (Brenner, 1963):

$$\vec{F}_D = -\overset{=T}{f}_p \cdot \vec{v}_p \tag{2a}$$

In the continuum limit ($Kn \to 0$), Brenner (1963) showed that the resistance to pure translational motion (without rotation) exerted by an incompressible fluid for a given particle shape may be expressed along principal directions, along which the motion is isotropic. Using this formalism and the method of Kirkwood and Riseman (1948), and extensions therein (Chen et al., 1984; Rotne & Prager, 1969; Yamakawa, 1970), $\overset{=T}{f}_p$ may be computed for particles of arbitrary shape consisting of point contacting spherical elements in the continuum regime (Corson, 2018; Corson et al., 2017c; Happel & Brenner, 2012). The use of the complete translational friction tensor for computing $\vec{F}_D$, though rigorous, often offers no more accuracy than using a scalar friction factor f_p^T that is orientation averaged for slight to moderately non-spherical shapes and is often considered to be an adequate approximation for shapes that do not have a preferred orientation when suspended in the gas phase (absence of aligning forces that are typically electrical or gravitational in origin):

$$\vec{F}_D = -f_p^T \vec{v}_p \tag{2b}$$

For spheres, f_p^T is derived analytically by solving for the drag on a sphere moving at a constant speed (without considering rotation) through a stagnant, infinite fluid medium at low speeds, commonly known as Stokes law (Friedlander, 2000):

$$Kn \to 0 : f_p^T = 6\pi\mu_g a_p \tag{3a}$$

Here, μ_g is the viscosity of the background gas. Eq. (3a) has also been generalized for arbitrary shapes by replacing the particle radius a_p with the particle capacitance/hydrodynamic radius R_h (Douglas et al., 1994; Hubbard & Douglas, 1993) that can be calculated for particles of any shape using algorithms described elsewhere (Given et al., 1997; Gopalakrishnan et al., 2011; Zhou et al., 1994):

$$Kn \to 0 : f_p^T = 6\pi\mu_g R_h \tag{3b}$$

In the free molecular limit of momentum transfer ($Kn \to \infty$), Rohatschek and Zulehner (1987) extend the formalism of Happel and Brenner (2012) and derive a functional form for $\overset{=T}{f}_p$. Larriba and Fernandez de la Mora (2012) rigorously show the exact form of $\overset{=T}{f}_p$ for cylinders and particles made up of point contacting spheres. From an experimental point of view, the measurement of orientation averaged diffusion constant D_p or particle electrical mobility ζ_p allows the inference of f_p^T directly as mentioned before. Sensitive experimental observables are not known currently to infer the elements of $\overset{=T}{f}_p$ for complex shapes and thus, serve as a practical reason for the usage of f_p^T widely. For a spherical particle in the free molecular regime f_p^T was derived by Epstein (1924):

$$Kn \to \infty : f_p^T = \frac{8}{3}\frac{\mu_g}{\lambda_g}\xi\pi a_p^2 \tag{4a}$$

ξ is a dimensionless coefficient, approximately equal to 1.36 as confirmed via prior experimental measurements (Millikan, 1923; Rader, 1990; Ku & de la Mora, 2009; Hogan & Fernandez de la Mora, 2011; Larriba et al., 2011), to accommodate the scattering of momentum of gas molecules upon reflection from the surface of the particle. For non-spherical particles, eq. (4a) is generalized in terms of the momentum transfer collision cross-section Ω_p of the particle (Chapman & Cowling, 1991; McDaniel & Mason, 1973; Vincenti & Kruger, 1975):

$$Kn \to \infty : f_p^T = \frac{8}{3}\frac{\mu_g}{\lambda_g}\Omega_p \tag{4b}$$

Zhang et al. (2012) proposed the "projected area approximation" to estimate $\Omega_p \approx \xi PA$ and found good agreement between eq. (4b) and Direct Simulation Monte Carlo (DSMC) calculations of f_p^T, also confirmed by the calculations of Corson et al. (2017c) using an extension of the Kirkwood-Risemann approach. Eq. (3) and eq. (4) establish the continuum and free molecular limits, respectively, of f_p^T for spheres and arbitrary shapes. For molecular ions in the gas phase ($Kn \gg 1$), $f_p^T = \frac{z_p e}{\zeta_p}$ is calculated from experimentally determined ion mobilities. Alternately, Larriba and co-workers (Larriba & Hogan, 2013a, 2013b; Shrivastav et al., 2017; Larriba-Andaluz & Prell, 2020; Larriba-Andaluz & Carbone, 2021), have developed IMoS (Coots et al., 2020) – a computationally efficient platform for computing Ω_p in the free molecular regime using MD simulations including gas molecule-particle collision physics, gas molecule rotation, particle-molecule dipole interactions and external electric fields, enabling the usage of eq. (4b) for ions and macromolecules of any shape or structure. In the intermediate, finite Kn transition regime of momentum transfer, a slip correction factor developed by fitting experimentally obtained f_p^T is used (Cunningham, 1910; Davies, 1945):

$$f_p^T(Kn) = \frac{6\pi\mu_g a_p}{1+\alpha_1\left(\alpha_2 + Kn\cdot e^{-\frac{\alpha_3}{Kn}}\right)} \tag{5a}$$

$\alpha_1, \alpha_2, \alpha_3$ are gas-specific coefficients summarized by Rader (1990). Eq. (5a) has been tested and been shown to be accurate to particles of size down to ~1.1 nm (Ku & de la Mora, 2009; Larriba et al., 2011) and has been extended to arbitrary shaped particles as well (Dahneke, 1973a, 1973b, 1973c; Gopalakrishnan et al., 2015b; Thajudeen, Jeon, & Hogan, 2015; Zhang et al., 2012) with *Kn* defined in terms of R_h and *PA*:

$$f_p^T(Kn) = \frac{6\pi\mu_g R_h}{1+\alpha_1\left(\alpha_2 + Kn\cdot e^{-\frac{\alpha_3}{Kn}}\right)} \tag{5b}$$

Eq. (5b) agrees well with the calculations of f_p^T for agglomerates consisting of point contacting spheres using an extension of the continuum Kirkwood-Risemann approach (Kirkwood & Riseman, 1948) to the finite *Kn* transition regime by Corson et al. (2017c) – the complete $\overset{=T}{f}_p$ for particles of arbitrary shape can also be computed using this approach, expanding the level of detail that can be accommodated in LD using eq. (1). An analytic expression for f_p^T valid specifically for DLCA aggregates has also been proposed by Corson et al. (2017a). Equation (3)–5 represent a complete set of f_p^T expressions valid for the entire *Kn* regime for computing $\overrightarrow{F}_D$ using eq. (2b) for pure translation of aerosol particles of known shape; wherever the complete translation friction factor tensor $\overset{=T}{f}_p$ is available, eq. (2a) may be used as well in trajectory simulations.

2.3. Hydrodynamic drag force $\overrightarrow{F}_D$ in dense particle concentration regimes

In Section 2.2, we summarized $\overset{=T}{f}_p$ calculation methodologies and f_p^T expressions for the modeling of momentum transfer onto an aerosol particle at low concentrations wherein the average inter-particle distance $n_p^{-\frac{1}{3}}$ is much larger than any other length scales: $n_p^{-\frac{1}{3}} \gg \lambda_g, l_p$; n_p is the particle number concentration. In other words, the particle volume fraction $\eta_v = n_p l_p^3 \to 0$ and the aerosol may be considered 'dilute'. For reference, dilute ambient, industrial or laboratory sub-micron aerosols often have $\eta_v \tilde{} 10^{-6} - 10^{-4}$ and particle-particle interactions may be taken to be binary and that the drag experienced by a single particle is not significantly influenced by the presence of other particles. A short summary of Corson et al.'s approach (Corson et al., 2017a, 2017b, 2017c, 2018a, 2018b; Corson, 2018) to compute $\overrightarrow{F}_D$ in the case of dense aerosols, wherein the particles occupy a non-trivial fraction of the system volume (i.e.) finite η_v is presented here. At high pressures and/or high concentrations, such as those found in explosions/detonations or fuel rich flames (see work by Sorensen et al. (Dhaubhadel et al., 2009; Dhaubhadel et al., 2012; Nepal et al., 2013; Nepal et al., 2015),) where the particles occupy a significant fraction of the system volume ($\eta_v > \tilde{} 10^{-2}$), the assumption that a particle is isolated and away from any surfaces/other particles in a fluid of infinite extent becomes moot. It becomes necessary to account for the perturbation of the gas flow around individual particles by the presence of other particles (i.e.) account for the finite η_v effects in the calculation of $\overset{=T}{f}_p$ or f_p^T. In the continuum regime of momentum transfer ($Kn \to 0$), particle trajectory simulations accounting for multi-body hydrodynamic interactions have been realized by neglecting particle inertia from eq. (1): $0 = \overrightarrow{F}_D + \overrightarrow{F}_B + \overrightarrow{F}_{ext}$. Stokesian Dynamics methods (Brady & Bossis, 1988; Brady et al., 1988; Brady & Sierou, 2001) use linear superposition to compute the resultant fluid flow field around an ensemble of interacting particles by exploiting the linearity of the underlying fluid flow equations in the limit of $Re_p \to 0, Kn \to 0$ and with no-slip boundary conditions: $0 = \mu_g \nabla^2 \overrightarrow{v}_g$. In the finite *Kn* transition regime of momentum transfer, Corson et al. (2018b) describe the calculation of $\overrightarrow{F}_D$ on a single particle including the perturbation of the fluid flow by the presence of other particles in the vicinity. This method allows the accounting of the non-negligible particle inertia $\left(m_p \frac{d\overrightarrow{v}_p}{dt}\right)$ while carrying out trajectory simulations of aerosol particle motion in dense environments. For illustration, we describe a calculation of the drag force on *N* identical, hydrodynamically interacting spheres in a gas here, that will later be utilized for the case study on aerosol coagulation described in Section 3.2. The drag force on the i^{th} sphere $\overrightarrow{F}_i$ is expressed in terms of the perturbation tensor $\overset{=}{V}_{ij}$, that captures the perturbation of the fluid flow field around sphere *i* due to the presence of sphere *j*:

$$\overrightarrow{F}_i = -f_i \overrightarrow{v}_i - \sum_{j=1,\, j\neq i}^{N} \overset{=}{V}_{ij} . \overrightarrow{F}_j \tag{6a}$$

In the limit that sphere *j* is at infinitely far distance from sphere *i*, the components of $\overset{=}{V}_{ij}$ are trivially zero. The functional form of $\overset{=}{V}_{ij}(Kn)$ (eq. (6b)) in the transition regime was obtained by generalizing $\overset{=}{V}_{ij}(Kn \to 0)$ derived in the continuum regime (Rotne & Prager, 1969; Yamakawa, 1970) to include *Kn*-dependent slip at the surface of the particle by Corson et al. (2017c):

$$\overline{\overline{V}}_{ij}(Kn) = -\frac{q_2^{(i)}(r_{ij})}{\sqrt{2}}\frac{\vec{r}_{ij}\vec{r}_{ij}}{r_{ij}^2} - \frac{q_3^{(i)}(r_{ij})}{\sqrt{2}}\left(\overline{\overline{I}} - \frac{\vec{r}_{ij}\vec{r}_{ij}}{r_{ij}^2}\right) \tag{6b}$$

$q_2^{(i)}(r_{ij})$ and $q_3^{(i)}(r_{ij})$ are calculated using the methods of Corson et al. (Corson, 2018; Corson et al., 2017c, 2018b) and tabulated as a function of $Kn = \frac{\lambda_g}{a_p}$ therein; $\vec{r}_{ij} = \vec{r}_j - \vec{r}_i$. Treating $\overline{\overline{V}}_{ij}$ to be a known function of particle relative positions $\vec{r}_{ij}$ and Kn in the transition regime, eq. (6a) is expanded as a set of $3N$ linear equations to solve for the components of the drag force $\vec{F}_i = (F_{xi}, F_{yi}, F_{zi})$ in terms of the position $\vec{r}_i = (r_{xi}, r_{yi}, r_{zi})$ and velocities $\vec{v}_i = (v_{xi}, v_{yi}, v_{zi})$ of $i = 1 - N$ spheres ($f_p = 6\pi\mu_g a_p$ is the friction factor of a spherical particle of radius a_p, $V_{ij:xy}$ represents the xy dyadic of the tensor $\overline{\overline{V}}_{ij}$):

$$i = 1 - N : \begin{cases} F_{xi} = -f_p v_{xi} - \sum_{j=1,\, j\neq i}^{N} \left(V_{ij:xx}F_{xj} + V_{ij:xy}F_{yj} + V_{ij:xz}F_{zj}\right) \\ F_{yi} = -f_p v_{yi} - \sum_{j=1,\, j\neq i}^{N} \left(V_{ij:yx}F_{xj} + V_{ij:yy}F_{yj} + V_{ij:yz}F_{zj}\right) \\ F_{zi} = -f_p v_{zi} - \sum_{j=1,\, j\neq i}^{N} \left(V_{ij:zx}F_{xj} + V_{ij:zy}F_{yj} + V_{ij:zz}F_{zj}\right) \end{cases} \tag{7}$$

Eq. (7) is compactly written in matrix form as ($k, l = 1 - 3$ is used to denote the x, y, z components, respectively, $V_{ij:kl}$ represents the kl dyadic of the $\overline{\overline{V}}_{ij}$ tensor):

$$A_{3N\times 3N} X_{3N\times 1} = B_{3N\times 1} \tag{8a}$$

$$X_{3(i-1)+(k)} = F_{ki};\ B_{3(i-1)+(k)} = -f_p v_{ki};\ k = 1-3;\ i = 1-N \tag{8b}$$

$$i = 1 - N : \left\{ k = 1 - 3 : \left\{ F_{ki} = -f_p v_{ki} - \sum_{j=1,\, j\neq i}^{N} \sum_{l=1}^{3} V_{ij:kl}F_{lj} \right.\right. \tag{8c}$$

$$X_{3(i-1)+(k)} = -f_p v_{ki} - \sum_{j=1}^{N} \sum_{l=1}^{3} \left(1 - \delta_{ij}\right) V_{ij:kl} X_{3(j-1)+(l)} \tag{8d}$$

For clarity, eq. (8d) is expanded to explicitly show the system of linear equations to be solved to obtain the set of drag forces $\vec{F}_i$ on each particle $i = 1 - N$:

$$i = 1 - N : \left\{ k = 1 - 3 : \left\{ X_{3(i-1)+k} = -f_p v_{ki} - \sum_{j=1}^{N} \left(1 - \delta_{ij}\right)\left(V_{ij:k1}X_{3(j-1)+1} + V_{ij:k2}X_{3(j-1)+2} + V_{ij:k3}X_{3(j-1)+3}\right) \right.\right. \tag{9a}$$

$$i = 1 - N : \begin{cases} X_{3(i-1)+1} = -f_p v_{1i} - \sum_{j=1}^{N} \left(1 - \delta_{ij}\right)\left(V_{ij:11}X_{3(j-1)+1} + V_{ij:12}X_{3(j-1)+2} + V_{ij:13}X_{3(j-1)+3}\right) \\ X_{3(i-1)+2} = -f_p v_{2i} - \sum_{j=1}^{N} \left(1 - \delta_{ij}\right)\left(V_{ij:21}X_{3(j-1)+1} + V_{ij:22}X_{3(j-1)+2} + V_{ij:23}X_{3(j-1)+3}\right) \\ X_{3(i-1)+3} = -f_p v_{3i} - \sum_{j=1}^{N} \left(1 - \delta_{ij}\right)\left(V_{ij:31}X_{3(j-1)+1} + V_{ij:32}X_{3(j-1)+2} + V_{ij:33}X_{3(j-1)+3}\right) \end{cases} \tag{9b}$$

The coefficient matrix $A_{3N\times 3N}$ is then expressed compactly as:

$$A_{[3(i-1)+k][3(j-1)+l]} = \begin{cases} i = j \rightarrow \begin{cases} 1, & k = l \\ 0, & k \neq l \end{cases} \\ i \neq j \rightarrow V_{ij:kl} \end{cases} \tag{10a}$$

Finally, $X_{3N\times 1}$ is calculated by matrix inversion to calculate $\vec{F}_i = (F_{xi}, F_{yi}, F_{zi})$:

$$X_{3N\times 1} = A_{3N\times 3N}^{-1} B_{3N\times 1} \tag{10b}$$

In a dynamical simulation of a system of particles, particle position $\vec{r}_i(t)$ and velocity $\vec{v}_i(t)$ from the previous timestep are used to compute the drag force on the ith particle $\vec{F}_i$ as a function of $\vec{r}_i(t)$, $\vec{v}_i(t)$, Kn via eq. (10). For a system of polydisperse spheres or agglomerates, the calculation procedure remains the same but the number of equations to be solved scales as $3N$, where N is the total number of primary spheres in all the agglomerates combined, as described by Corson et al. (2018b). The solution to eq. (6a) using Corson et al.'s $\overline{\overline{V}}_{ij}$ for finite-Kn gas flow around an aerosol particle is an attractive approach for computing multi-body hydrodynamic

interactions in the momentum transfer transition regime, enabling the complete dynamical simulation of system of hydrodynamically coupled aerosol particles. In prior work on the coagulation of dense aerosols (Buesser et al., 2009; Heine & Pratsinis, 2007; Trzeciak et al., 2004), for example, particle-particle hydrodynamic interactions that are significant at $\eta_v > \tilde{}10^{-2}$ were neglected and may now be self-consistently included as demonstrated in Section 3.2. The complete friction tensor $\overset{=T}{f}_p$, relevant for non-spherical particles, can also be readily incorporated in this formalism to improve the accuracy of LD trajectory simulations. Future work that compares the predictions of particle coagulation rates or the evolution of the moments of the particle size distribution from dynamical simulations of dense aerosols will presumably place Corson et al.'s extended Kirkwood-Risemann method for hydrodynamic interactions on a firmer footing for widespread use. Lastly, hydrodynamic interactions between particles identically vanish in the free molecular limit $\overset{=}{V}_{ij}(Kn \to \infty) \to 0$ and eq. (6a) reduces to eq. (2a) exactly.

2.4. Stochastic brownian force $\vec{F}_B$

The stochastic force $\vec{F}_B$, representative of random thermal impulses experienced by the particle due to collisions with gas molecules, as a normally distributed random vector (of zero mean and specified variance in terms of the scalar friction factor f_p) is valid in the limit of $t_r \ll t_s$ for the unconfined motion of particles:

Table 1
Symbols used: $z_{1,2}$ is the elementary charges of particles (1, 2); e is the electron charge; ε_0 is the permittivity of vacuum; ε_r is the particle dielectric constant; r is the radial separation between (1, 2); $R_{1,2}$ is the radius of (1, 2); A is the particle Hamaker constant; m_1 is the mass of (1); $\vec{E}(\vec{r}_1(t),t)$ is a spatially and/or temporally varying electric field; $\vec{B}(\vec{r}_1(t),t)$ is a spatially and/or temporally varying magnetic field; local fluid velocity $\vec{v}_g(\vec{r}_1(t),t)$.

Description of $\vec{F}_1 = -\nabla\Phi(r)$ or $\vec{F}_1(\vec{r}_1(t),t)$
Coulomb interaction between point charges (1, 2); a spherical particle (1) and a point charge (2). For a detailed summary of ion-ion dipole interaction potentials, see Hiemenz and Rajagopalan (1997). $\Phi(r) = \frac{z_1 z_2 e^2}{4\pi\varepsilon_0 r}$ Applications: Ion-ion collisional recombination (unlike charged ions), Coulomb scattering (like charged ions), like or unlike charged spherical particle-ion diffusion charging.
Screened Coulomb interaction between a spherical particle (1) and a point charge (2). $\Phi(r) = \frac{z_1 z_2 e^2}{4\pi\varepsilon_0 r} e^{-\frac{r}{\lambda_D}}$ Applications: Screening of particle at high space charge concentrations, such as those in dusty plasmas and ionized gases, using a linearized Debye length $\lambda_D = \left(\frac{\varepsilon_0 k_B T_g}{n_i e^2}\right)^{\frac{1}{2}}$.
Image potential interaction between a spherical particle (1) and point mass ion (2). For a detailed discussion of the derivation of the image potential, see Jackson (1975); Jeans (1925). For a straightforward implementation of the method of images for the image potential interaction between two spherical particles (1, 2), see Soules (1990). For the combined Coulomb and image potential between a perfectly conducting point contact agglomerate particle (1) and a point mass ion (2), see Gopalakrishnan, Thajudeen, et al. (2013). $\Phi(r) = -\frac{1}{2}\frac{\varepsilon_r - 1}{\varepsilon_r + 1}\frac{z_2^2 e^2}{4\pi\varepsilon_0}\frac{a_p^3}{r^2 - a_p^2}$ Applications: Collisions between neutral particle and ions in the context of charging; strongest for conducting particles ($\varepsilon_r \to \infty$) and vanishes for dielectric particles ($\varepsilon_r \to 0$).
van der Waals potential interaction between two spherical particles (1, 2) valid for non-retarded van der Waals interaction between spherical particles only; inclusion of retardation effects leads to distance-dependent Hamaker constant A for specific particle material combinations. For a detailed summary of interaction potentials between particles of various shapes, see Hiemenz and Rajagopalan (1997). $\Phi(r) = -\frac{A}{6}\left[2R_1R_2\left(\frac{1}{f_1(R_1,R_2,r)} + \frac{1}{f_2(R_1,R_2,r)}\right) + \ln\left(\frac{f_1(R_1,R_2,r)}{f_2(R_1,R_2,r)}\right)\right]$ $f_1(R_1,R_2,r) = r^2 + 2R_1r + 2R_2r$ $f_2(R_1,R_2,r) = r^2 + 2R_1r + 2R_2r + 4R_1R_2$ Applications: Collisions between neutral particles in coagulation and condensation processes, particle-surface interactions in deposition, impaction, bounce and resuspension processes.
Gravity: $\vec{F}_1 = m_1\vec{g}$ Applications: Particle inertial settling time calculations, mechanical mobility calculations
External electric field: $\vec{F}_1(\vec{r}_1(t),t) = z_1 e\vec{E}(\vec{r}_1(t),t)$ Applications: Particle motion in applied electric fields, field chargers, differential mobility classifiers, electrostatic precipitators, dusty plasmas.
External magnetic field: $\vec{F}_1(\vec{r}_1(t),t) = z_1 e(\vec{v}_1 \times \vec{B}(\vec{r}_1(t),t))$ Applications: Particle motion in applied magnetic fields, dusty plasmas
Bulk fluid flow: Eq. (2a) can be generalized to include local fluid velocity $\vec{v}_g$ as $\vec{F}_D = -\overset{=T}{f}_p \cdot (\vec{v}_p - \vec{v}_g)$. For such instances, $\vec{F}_1 = \overset{=T}{f}_p \cdot \vec{v}_g$ is treated as an external force in eq. (1). Applications: Particle transport in internal/external flows, impactors, differential mobility classifiers, diffusion battery, flow devices.

$$\int_0^{t_r} \vec{F}_B(t')dt' = 0 \tag{11a}$$

$$\int_0^{t_r} \vec{F}_B(t_r) \cdot \vec{F}_B(t' - t_r)dt' = 6f_p k_B T_g \delta(t_r) \tag{11b}$$

More generally, the translation friction tensor $\overset{=T}{f}_p$ may be used to express co-variances of the stochastic force in terms of the tensor components f_{ij}^T (F_B^i is the i^{th} component of $\vec{F}_B$):

$$\int_0^{t_r} F_B^i(t_r)F_B^j(t' - t_r)dt' = 2\gamma_{ij}\delta(t_r) \tag{12a}$$

$$k_B T_g f_{ij}^T = \gamma_{il}\gamma_{lj} \tag{12b}$$

For Brownian motion encountered in aerosol and dusty plasma systems, a Gaussian thermal noise is an adequate model but it is conceivable that physically motivated non-Gaussian approximations for $\vec{F}_B(t)$ may be incorporated easily as well (Berkowitz et al., 1983; Ermak & Buckholz, 1980; Risken & Frank, 1996).

2.5. External forces $\vec{F}_{ext}$

Applications of LD simulations include the prediction of aerosol behavior under the action of external forces. By statistically averaging over an ensemble of particle trajectories, the effect of stochastic Brownian motion is filtered out to deduce the average behavior of particles in systems of interest. In this section, we summarize, by no means exhaustively, various external forces and possible applications in Table 1 for incorporation into dynamical simulations of a population of particles.

2.6. Numerical integration schemes for solving the Langevin equation of motion

Using the force terms described in Sections 2.2–2.5, a system of Langevin ODEs may be used to describe $N \geq 1$ particles by integrating in time explicitly. We discuss two time-stepping schemes for stochastic ODEs that have been widely implemented for simulating stochastic processes and may be considered well established.

2.6.1. First order time-stepping scheme

Ermak and Buckholz (1980) describe a first-order time-stepping scheme that is valid for arbitrary forms of $\vec{F}_{ext}$. In case of time varying external forces, it is necessary that they vary slower than the timescale t_{ext} over which the particles relax to a Maxwell-Boltzmann velocity distribution t_r (i. e.) $t_{ext} \gg t_r$. For the sake of clarity, we re-state eq. (1) for the motion of a particle undergoing translational motion moving under the influence of an arbitrary external force $\vec{F}_{ext}$ with a scalar friction factor f_p:

$$m_p \frac{d\vec{v}_p}{dt} = -f_p \vec{v}_p + \vec{F}_{ext} + \vec{F}_B \tag{13}$$

In Ermak and Buccholz's original paper, that has received over 300 citations since publication, three variants of a first order method were presented. Here, we state the particular variant in which the stochastic particle velocity and displacement fluctuations added to the deterministic part of the solution at each timestep have zero co-variance, (i. e.) $\vec{R}_v \cdot \vec{R}_r = 0$ and has produced excellent agreement with a wide range of aerosol diffusion experimental data for particle-ion collision kernel models developed using this numerical method in our prior work (Li et al., 2020; Li & Gopalakrishnan, 2021; Ouyang et al., 2012):

$$\vec{v}_p(t + \Delta t) = \vec{v}_p(t)e^{-\frac{f_p}{m_p}\Delta t} + \frac{\vec{F}_{ext}}{f_p}\left(1 - e^{-\frac{f_p}{m_p}\Delta t}\right) + \left(\frac{1}{3}\vec{R}_v \cdot \vec{R}_v\right)^{\frac{1}{2}} \begin{bmatrix} NRAND(0,1) \\ NRAND(0,1) \\ NRAND(0,1) \end{bmatrix} \tag{14a}$$

$$\vec{R}_v \cdot \vec{R}_v = \frac{3k_B T_g}{m_p}\left(1 - e^{-2\frac{f_p}{m_p}\Delta t}\right) \tag{14b}$$

$$\vec{r}_p(t+\Delta t) = \vec{r}_p(t) + \frac{m_p}{f_p}\left(\vec{v}_p(t+\Delta t) + \vec{v}_p(t) - 2\frac{\vec{F}_{ext}}{f_p}\right)\left(\frac{1-e^{-\frac{f_p}{m_p}\Delta t}}{1+e^{-\frac{f_p}{m_p}\Delta t}}\right) + \frac{\vec{F}_{ext}}{f_p}\Delta t + \left(\frac{1}{3}\vec{R}_r\cdot\vec{R}_r\right)^{\frac{1}{2}}\begin{bmatrix} NRAND(0,1) \\ NRAND(0,1) \\ NRAND(0,1)\end{bmatrix} \tag{14c}$$

$$\vec{R}_r\cdot\vec{R}_r = \frac{6m_pk_BT_g}{f_p^2}\left(\frac{f_p}{m_p}\Delta t - 2\frac{1-e^{-\frac{f_p}{m_p}\Delta t}}{1+e^{-\frac{f_p}{m_p}\Delta t}}\right) \tag{14d}$$

Here, $NRAND(0,1)$ is a normally distributed random number with a mean of 0 and variance of 1; $\vec{R}_v$ and $\vec{R}_r$ are normally distributed random vectors of velocity and displacement, respectively, of mean zero and variance given by eq. (14b) and eq. (14d), added to capture the particle's Brownian motion. The timestep Δt used for simulation needs to be carefully determined to minimize loss of accuracy in computed trajectories. In a typical simulation, the order of magnitude of the Δt may be estimated by comparing the displacement steps due to the deterministic and stochastic forces:

$$\Delta t \sim \min\left(\frac{l_p f_p}{\left|\vec{F}_{ext}\right|}, \frac{l_p^2 f_p}{6k_BT_g}\right) \tag{15}$$

For a specific system, Δt may be estimated by progressively reducing the Δt calculated using eq. (15) as a starting point, until the calculate trajectories or calculated statistical quantities are no longer sensitive to Δt. This aspect will be demonstrated in Sections 2.6.3, 3.1 and 3.2.

2.6.2. Fourth order time-stepping scheme

Kasdin (1995) describes a fourth-order Runge-Kutta (RK) method, that has received 45 citations since publication and is widely used across many fields to model driven-dissipative systems (Dong et al., 2011), for the integration of linear stochastic ODEs of the form of eq. (1) or 13, restated as a system of 2 first-order ODEs (16a and 16b), written in matrix form (16c):

$$\frac{d\vec{r}_p}{dt} = \vec{v}_p \tag{16a}$$

$$\frac{d\vec{v}_p}{dt} = -\frac{f_p^T}{m_p}\vec{v}_p + \frac{\vec{F}_{ext}}{m_p} + \frac{\vec{F}_B}{m_p} \tag{16b}$$

$$\dot{\boldsymbol{X}} = \boldsymbol{F}(\boldsymbol{X},t) + \boldsymbol{\Pi}(t) \tag{16c}$$

$\boldsymbol{X} = \begin{pmatrix}\vec{r}_p \\ \vec{v}_p\end{pmatrix}$, $\boldsymbol{F}(\boldsymbol{X},t) = \begin{pmatrix}\vec{v}_p \\ -\frac{f_p^T\vec{v}_p}{m_p} + \frac{\vec{F}_{ext}}{m_p}\end{pmatrix}$, $\boldsymbol{\Pi}(t) = \begin{pmatrix}0 \\ \frac{\vec{F}_B}{m_p}\end{pmatrix}$ are, respectively, the solution, deterministic and stochastic column vectors (shown in **bold** font). A known point in the phase-space $\boldsymbol{X}(t)$ is used to calculate the solution at $\boldsymbol{X}(t+\Delta t)$:

$$\boldsymbol{X}(t+\Delta t) = \boldsymbol{X}(t) + \alpha_1\boldsymbol{k}_1 + \alpha_2\boldsymbol{k}_2 + \alpha_3\boldsymbol{k}_3 + \alpha_4\boldsymbol{k}_4 \tag{17a}$$

$$\boldsymbol{k}_1 = \Delta t\boldsymbol{F}(\boldsymbol{X}(t),t) + \Delta t D^{\frac{1}{2}}\begin{pmatrix}0 \\ NRAND(0,1)\end{pmatrix} \tag{17b}$$

$$j=2,\ 3,\ 4:\ \boldsymbol{k}_j = \Delta t\boldsymbol{F}\left(\boldsymbol{X}(t) + \sum_{i=1}^{j-1}a_{ji}\boldsymbol{k}_i, t + c_j\Delta t\right) + \Delta t\left(Dq_j\right)^{\frac{1}{2}}\begin{pmatrix}0 \\ NRAND(0,1)\end{pmatrix} \tag{17c}$$

Coefficients a_{ji}, α_i, q_j are tabulated in Table S2, *SI*; $D = \frac{2f_p^Tk_BT_g}{\Delta t}$ and $c_j = \sum_{i=1}^{j-1}a_{ji}$. Similar to eq. (15), Δt is estimated by comparing the velocity step, deterministic and stochastic forces:

$$\Delta t = \min\left(\frac{l_p}{\left|\vec{v}_p\right|}, \sqrt{\frac{m_pl_p}{\left|\vec{F}_{ext}\right|}}, \left(\frac{l_p^2m_p^2}{6f_pk_bT_gq_4}\right)^{\frac{1}{3}}\right) \tag{18}$$

Lastly, Kasdin and Stankievech (2009) describe a RK method for coupled non-linear stochastic ODEs that is potentially useful for

the incorporation of the full translational friction tensor $\overset{=T}{f}_p$ in eq. (1).

2.6.3. Example on the usage of LD to predict the settling time distribution of sub-micron spherical aerosol particles in still air, at room temperature

Parameters: Particle density $\rho_p = 1000\frac{kg}{m^3}$; gas pressure $p_g = 101325\,Pa$; gas temperature $T_g = 300\,K$; viscosity of air $\mu_g = 1.8\times 10^{-5} Pa.s$; particle mass $m_p = \rho_p\frac{\pi}{6}d_p^3$; d_p is particle diameter varied between 10 and 1000 nm. Scalar friction factor f_p^T calculated using eq. (5a) with $\alpha_1 = 1.250, \alpha_2 = 0.4, \alpha_3 = 1.1$ corresponding to air (Rader, 1990).

Governing LD ODE:

$$m_p\frac{d\vec{v}_p}{dt} = -f_p^T\vec{v}_p + m_p\vec{g} + \vec{F}_B \tag{19a}$$

Eq. (20a) is integrated using the first order method (eq. (14), referred to as the EB method hereon) in a 3D cartesian coordinate system to the particle's motion tracked from a height of $z = H$ and gravity acts along the vertical direction: $\vec{g} = -\left(9.8\frac{m}{s^2}\right)\hat{k}$, subject to initial conditions:

$$\vec{r}_p(t=0) = 0\hat{i} + 0\hat{j} + H\hat{k} \tag{19b}$$

$$\vec{v}_p(t=0) = \left(\frac{k_BT_g}{m_p}\right)^{\frac{1}{2}}\left[\hat{i}NRAND(0,1) + \hat{j}NRAND(0,1) + \hat{k}NRAND(0,1)\right] \tag{19c}$$

Eq. (19c) may be recognized as the sampling of the particle's 3D velocity from a Maxwell-Boltzmann distribution for each component, with a mean of zero and variance of $\frac{k_BT_g}{m_p}$, assuming thermal equilibrium between the settling particle and the gas. The simulation is advanced using a variable time step of $\Delta t(s)$ (eq. (20) below) until the particle reaches the bottom surface defined by $z = 0$ (i. e.) $z \le 0$ and is considered to have settled from a height of $H = 0.1\ m$ (without considering particle bounce off of the surface):

$$\Delta t(s) = 0.01\cdot\min\left(\frac{z^2f_p}{6k_BT_g}, \frac{zf_p}{m_pg}\right) \tag{20}$$

For a chosen particle size, $N_T = 1000$ trials of particle settling are run to create a histogram of settling times shown in Fig. 1a for $d_p = 500\ nm$. By averaging over N_T trials, an average settling time $t_S = \frac{1}{N_T}\sum_{i=1}^{N_T} t_{S,i}$ and the standard deviation $\sigma_S = \sqrt{\frac{1}{N_T-1}\sum_{i=1}^{N_T}(t_{S,i}-t_S)^2}$ are calculated and plotted in Fig. 1b as a function of d_p; $t_{S,i}$ is the settling time calculated in the i-th trial. Fig. 2 shows sample trajectories for $d_p = 10, 100, 1000$ nm, calculated using the EB method, to illustrate the effect of stochastic Brownian motion on the settling of an aerosol particle. LD is a useful tool for sampling and visualizing particle trajectories that are the convolutions of various underlying dissipative (drag), deterministic (gravity) and stochastic (thermal kicks) force distributions and for calculating the average statistical transport properties of an ensemble of particles, and as illustrated by the particle settling time calculation in this example. The online *Supplementary Information* (SI) accompanying this tutorial article includes a MATLAB® (.m) implementation of the 3D EB method ("EB_3D_Settling.m") for simulating this example with comments.

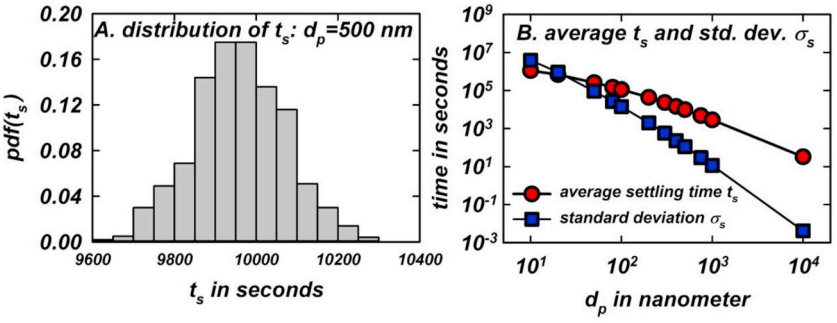

Fig. 1. A. Histogram of gravitational settling times for a $d_p = 500\ nm$ spherical particles in still air. The settling times are well described by a generalized extreme value distribution with parameters $\mu = 9917.68,\ k = -0.2593, \sigma = 111.708$. Other parameters used in the trajectory simulations are noted in Sec. 2.6.3. **B.** Plot of average settling time t_s and standard deviation σ_s as a function of particle diameter d_p.

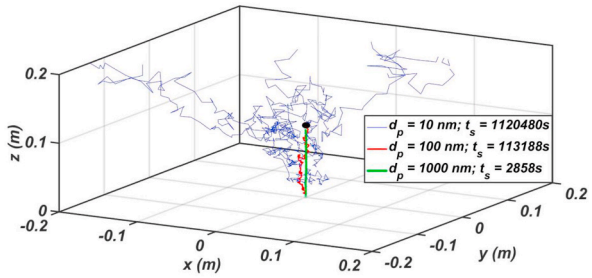

Fig. 2. Calculated particle trajectories for the gravitational settling of 10, 100, 1000 *nm* spherical particles in still air. The starting point is indicated; it is seen that the 1000 nm particle has an average settling time t_S~2900 *s* dominated by gravitation force, while the 10 *nm* particle wanders considerably before settling down with t_S~10^6 *s*. The 100 *nm* particle has aspects of both deterministic settling and stochastic Brownian motion with a t_S~10^5 *s*.

3. Demonstrations

3.1. Modeling of particle-ion diffusion charging collision kernel

Diffusion charging is a mass transfer process in which gas-phase ions undergo combined diffusional and electrostatic motion to impinge upon particles at low speeds and transfer charge. This process, ubiquitous in the atmosphere as well as used for imparting a known charge distribution to generated/sampled sub-micron aerosols before electrical mobility-based classification (Knutson & Whitby, 1975), has been investigated by Gopalakrishnan et al. using LD simulations (Chahl & Gopalakrishnan, 2019; Gopalakrishnan et al., 2013a, 2013b, 2015a; Gopalakrishnan & Hogan, 2012; Li et al., 2020; Li & Gopalakrishnan, 2021; Ouyang et al., 2012). In this demonstration, we describe the physical problem only briefly, focus on the computational methodology and refer the interested reader to Chahl and Gopalakrishnan (2019) and Gopalakrishnan and Hogan (2012) for a detailed discussion of the simulation results and the underlying physics.

The rate R_{pi} at which particle-ion collisions that result in the particle charge z_p being modified as $z_p \rightarrow z_p + z_i$, where z_i is the charge carried by the ion, may be calculated as $R_{pi} = \beta_{pi} n_p n_i$; here, n_p is the concentration of particles carrying z_p charges and n_i is the gas-phase ion concentration.β_{pi} has modeled or theorized by various approaches (Bricard, 1962; Fuchs, 1963; Marlow, 1980; Hoppel & Frick, 1986; Lushnikov & Kulmala, 2004; D'Yachkov et al., 2007; Gatti & Kortshagen, 2008; Lopez-Yglesias & Flagan, 2013; Gopalakrishnan et al., 2015a; Sharma et al., 2019), including LD that we focus upon here. β_{pi} is calculated using LD by simulating the ion motion in the vicinity of an aerosol particle (assumed to be at rest) including the particle-ion Coulomb interaction potential $\Phi_{pi} = \frac{z_p z_i e^2}{4\pi\varepsilon_0 \left| \vec{r}_i - \vec{r}_p \right|}$ and $\vec{F}_D$, $\vec{F}_B$ described previously. By calculating the average particle-ion collision time $\tau(s)$ in a periodic domain of volume L^3 (m^3), Chahl and Gopalakrishnan (2019) infer $\beta_{pi}\left(\frac{m^3}{s}\right) = \frac{L^3}{\tau}$ and use scaling analysis to build a model for β_{pi}, expressed in a non-dimensional form. We show the intermediate steps to develop a model for β_{pi} and start by non-dimensionalizing the EB solution (eq. (14)) to the LD ODE for a single ion colliding with a stationary particle:

$$m_i \frac{d\vec{v}_i}{dt} = -f_i \vec{v}_i - \nabla \Phi_{pi} + \vec{F}_B \tag{21}$$

To scale distances the particle radius a_p is used, the ion relaxation time in the gas $\frac{m_i}{f_i}$ is used as a unit for time (note that f_i has units of $\frac{kg}{s}$) and $\frac{a_p f_i}{m_i}$ is used as a reference velocity. With these choices, the non-dimensional form of eq. (14) is written as follows, with an * symbol used to denote that the involved quantities are unitless:

$$\vec{v}^{\,*}_i(t^* + \Delta t^*) = \vec{v}^{\,*}_i(t^*) e^{-\Delta t^*} - \frac{m_i}{a_p f_i^2} \nabla \Phi_{pi} \left(1 - e^{-\Delta t^*}\right) + \left(\frac{1}{3} \vec{R}^{\,*}_v \cdot \vec{R}^{\,*}_v\right)^{\frac{1}{2}} \begin{bmatrix} NRAND(0,1) \\ NRAND(0,1) \\ NRAND(0,1) \end{bmatrix} \tag{22a}$$

$$\vec{R}^{\,*}_v \cdot \vec{R}^{\,*}_v = 3 \frac{m_i k_B T_g}{a_p^2 f_i^2} \left(1 - e^{-2\Delta t^*}\right) \tag{22b}$$

$$\vec{r}^{\,*}_i(t^* + \Delta t^*) = \vec{r}^{\,*}_i(t^*) + \left(\vec{v}^{\,*}_i(t^* + \Delta t^*) + \vec{v}^{\,*}_i(t^*) + 2 \frac{m_i}{a_p f_i^2} \nabla \Phi_{pi}\right) \left(\frac{1 - e^{-\Delta t^*}}{1 + e^{-\Delta t^*}}\right) - \frac{m_i}{a_p f_i^2} \nabla \Phi_{pi} \Delta t^* + \left(\frac{1}{3} \vec{R}^{\,*}_r \cdot \vec{R}^{\,*}_r\right)^{\frac{1}{2}} \begin{bmatrix} NRAND(0,1) \\ NRAND(0,1) \\ NRAND(0,1) \end{bmatrix} \tag{22c}$$

$$\vec{R}^{*}_{r} \cdot \vec{R}^{*}_{r} = 6\frac{m_i k_B T_g}{a_p^2 f_i^2}\left(\Delta t^{*} - 2\frac{1-e^{-\Delta t^{*}}}{1+e^{-\Delta t^{*}}}\right) \tag{22d}$$

Eq. (22) contains two dimensionless combinations of physical variables that are recognized as independent parametric inputs for the calculation of β_{pi}:

$$\frac{m_i k_B T_g}{a_p^2 f_i^2} = \left[\left(\frac{\sqrt{m_i k_B T_g}}{f_i}\right) \Big/ a_p\right]^2 \tag{23a}$$

Chahl and Gopalakrishnan (2019), as well as previously in this article, discussed that $\left(\frac{\sqrt{m_i k_B T_g}}{f_i}\right)$ is the mean persistence path λ_{mpp} of the ion as it collides with a particle due to combined Brownian and electrostatic motion while experiencing dissipative drag forces exerted by the gas medium. Eq. (23a) represents a quantity that is ratio between λ_{mpp} and the collision length scale a_p and is recognized as the particle-ion diffusive Knudsen number Kn_D:

$$Kn_D = \frac{\sqrt{m_i k_B T_g}}{f_i a_p}\frac{\eta_c(\Psi_E)}{\eta_f(\Psi_E)} \tag{23b}$$

Two functions $\eta_c(\Psi_E), \eta_f(\Psi_E)$ are added to the definition of Kn_D to ensure that in the continuum regime ($Kn_D \to 0$) and the free molecular regime ($Kn_D \to \infty$), expressions constructed for non-dimensional β_{pi} converge to the appropriate analytical expressions, as described in detail by Chahl and Gopalakrishnan (2019). It is sufficient to note here that $\eta_c(\Psi_E), \eta_f(\Psi_E)$ can be calculated analytically or numerically as a function of Ψ_E (eq. (24c) below). The other combination that appears in eq. (22) is:

$$-\frac{m_i}{a_p f_i^2}\nabla\Phi_{pi} = -\frac{m_i}{a_p f_i^2}\nabla\left(\frac{z_p z_i e^2}{4\pi\varepsilon_0\left|\vec{r}_i - \vec{r}_p\right|}\right) = \frac{m_i}{a_p f_i^2}\left(\frac{z_p z_i e^2}{4\pi\varepsilon_0\left|\vec{r}_i - \vec{r}_p\right|^2}\right)\frac{\left(\vec{r}_i - \vec{r}_p\right)}{\left|\vec{r}_i - \vec{r}_p\right|} = \frac{m_i}{a_p f_i^2}\left(\frac{z_p z_i e^2}{4\pi\varepsilon_0 a_p^2}\right)\frac{\left(\vec{r}^{*}_i - \vec{r}^{*}_p\right)}{\left|\vec{r}^{*}_i - \vec{r}^{*}_p\right|^3} \tag{24a}$$

By recognizing $-\frac{z_p z_i e^2}{4\pi\varepsilon_0 a_p}$ as an order of magnitude of the particle-ion electrostatic potential energy and by multiplying and dividing by $k_B T_g$ (the ion's mean kinetic/thermal energy), we rewrite eq. (24a) and recognize the definition of the dimensionless parameter Ψ_E (eq. (24c)):

$$-\frac{m_p}{a_p f_i^2}\nabla\Phi_{pi} = -\frac{m_i k_B T_g}{a_p f_i^2}\left(-\frac{z_p z_i e^2}{4\pi\varepsilon_0 a_p k_B T_g}\right)\frac{\left(\vec{r}^{*}_i - \vec{r}^{*}_p\right)}{\left|\vec{r}^{*}_i - \vec{r}^{*}_p\right|^3} = -\left(Kn_D^2\frac{\eta_f^2}{\eta_c^2}\right)\Psi_E\frac{\left(\vec{r}^{*}_i - \vec{r}^{*}_p\right)}{\left|\vec{r}^{*}_i - \vec{r}^{*}_p\right|^3} \tag{24b}$$

$$\Psi_E = -\frac{z_p z_i e^2}{4\pi\varepsilon_0 a_p k_B T_g} \tag{24c}$$

$$\eta_c(\Psi_E) = \frac{\Psi_E}{1-e^{-\Psi_E}} \tag{24d}$$

$$\eta_f(\Psi_E) = \begin{cases} e^{\Psi_E}, \ \Psi_E \le 0 \\ 1+\Psi_E, \Psi_E \ge 0 \end{cases} \tag{24e}$$

Ψ_E is a comparison of the ion's electrostatic potential energy to kinetic energy. $\Psi_E = 0$ represents hard sphere motion of the ion without the influence of any potential interactions, while $\Psi_E \gg \frac{3}{2}$ represents motion that is strongly influenced by the particle-ion electrostatic force; $\Psi_E > 0$ represents collisions between unlike charged particles and ions and vice versa. Eq. (22) may be rewritten in terms of Ψ_E, Kn_D as:

$$\vec{v}^{*}_i(t^{*}+\Delta t^{*}) = \vec{v}^{*}_i(t^{*})e^{-\Delta t^{*}} - \Psi_E Kn_D^2\frac{\eta_f^2}{\eta_c^2}\frac{\left(\vec{r}^{*}_i - \vec{r}^{*}_p\right)}{\left|\vec{r}^{*}_i - \vec{r}^{*}_p\right|^3}\left(1-e^{-\Delta t^{*}}\right) + \left(\frac{1}{3}\vec{R}^{**}_v \cdot \vec{R}^{**}_v\right)^{\frac{1}{2}}\begin{bmatrix} NRAND(0,1) \\ NRAND(0,1) \\ NRAND(0,1) \end{bmatrix} \tag{25a}$$

$$\vec{R}^{*}_v \cdot \vec{R}^{*}_v = 3Kn_D^2\left(1-e^{-2\Delta t^{*}}\right) \tag{25b}$$

$$\vec{r}^{\,*}_i(t^*+\Delta t^*) = \vec{r}^{\,*}_i(t^*) + \left(\vec{v}^{\,*}_i(t^*+\Delta t^*) + \vec{v}^{\,*}_i(t^*) + 2\Psi_E Kn_D^2 \frac{\eta_f^2}{\eta_c^2} \frac{\left(\vec{r}^{\,*}_i - \vec{r}^{\,*}_p\right)}{\left|\vec{r}^{\,*}_i - \vec{r}^{\,*}_p\right|^3} \right) \left(\frac{1-e^{-\Delta t^*}}{1+e^{-\Delta t^*}}\right) - \Psi_E Kn_D^2 \frac{\eta_f^2}{\eta_c^2} \frac{\left(\vec{r}^{\,*}_i - \vec{r}^{\,*}_p\right)}{\left|\vec{r}^{\,*}_i - \vec{r}^{\,*}_p\right|^3} \Delta t^* + \left(\frac{1}{3}\vec{R}^{\,*}_r \cdot \vec{R}^{\,*}_r\right)^{\frac{1}{2}} \begin{bmatrix} NRAND(0,1) \\ NRAND(0,1) \\ NRAND(0,1) \end{bmatrix} \tag{25c}$$

$$\vec{R}^{\,*}_r \cdot \vec{R}^{\,*}_r = 6Kn_D^2 \left(\Delta t^* - 2\frac{1-e^{-\Delta t^*}}{1+e^{-\Delta t^*}}\right) \tag{25d}$$

The ion is initialized on the surface of the periodic box one on of the six faces chosen randomly with a velocity sampled randomly from a Maxwell-Boltzmann distribution:

$$\vec{v}^{\,*}_i(t^*=0) = Kn_D\left[\hat{i}NRAND(0,1) + \hat{j}NRAND(0,1) + \hat{k}NRAND(0,1)\right] \tag{26}$$

Eq. (25) represents the non-dimensional velocity $\vec{v}^{\,*}_i(t^*)$ and position $\vec{r}^{\,*}_i(t^*)$ of the ion that is tracked in a periodic domain of side L^* with a spherical particle of non-dimensional radius 1 at the origin $\vec{r}^{\,*}_p(t) = (0,0,0)$ as a function of Ψ_E, Kn_D as inputs. Collisions are detected when $\left|\vec{r}^{\,*}_i - \vec{r}^{\,*}_p\right| \leq 1$ and the ion position and velocity are re-initialized for simulating N_T trials as desired (typically, N_T~2000 yields good statistical confidence on the calculated ensemble averages). Lastly, β_{pi} is reduced to a dimensionless form H (Chahl & Gopalakrishnan, 2019; Gopalakrishnan, Thajudeen, et al., 2013; Gopalakrishnan & Hogan, 2012; Li et al., 2020; Li & Gopalakrishnan, 2021; Ouyang et al., 2012):

$$H = \frac{\beta_{pi} m_i}{f_i a_p^3} \frac{\eta_c}{\eta_f^2} \tag{27a}$$

In total, the functional dependence (eq. (27b)) of β_{pi} on the radius a_p and elementary charge z_p of a conducting particle ($\varepsilon_r \to \infty$), ion mass m_i, ion scalar friction factor f_i (that is dependent on gas pressure p_g) and gas temperature $k_B T_g$ is expressed compactly in non-

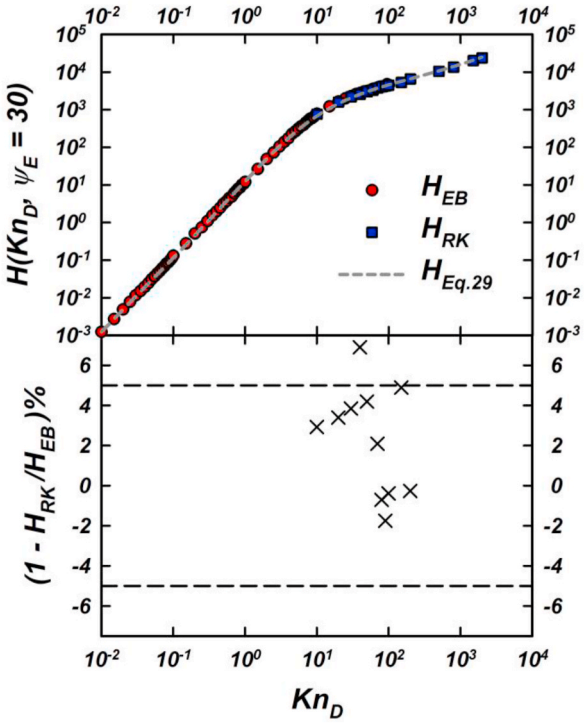

Fig. 3. **A.** $H(Kn_D, \Psi_E)$ Calculated using the EB method (red filled circles) and RK method (blue filled squares) shown along with the prediction of the model (grey dashed line) developed by Chahl and Gopalakrishnan (2019) given by eq. (29) for $\Psi_E = 30$. Simulation parameters, $L^* = 4000$, $T^* = 0.005$. **B.** % difference between H Calculated using the EB method (H_{EB}) and the RK method (H_{RK}) for $10 \leq Kn_D \leq 200$. Reference lines at ± 5% are included.

dimensional form (eq. (27c)):

$$\beta_{pi} = \beta_{pi}\left(a_p, m_i, f_i, k_B T_g, z_p\right) \tag{27b}$$

$$H = H(Kn_D, \Psi_E) \tag{27c}$$

It is necessary that H inferred from LD simulations be insensitive to the simulation parameters L^* and Δt^* to be physically valid and are selected as follows (Chahl & Gopalakrishnan, 2019):

$$L^* = \max\left(500, \frac{400}{3}\Psi_E\right) \tag{28a}$$

$$\Delta t^* = T^* \min\left(\frac{\left|\overrightarrow{r}_i^* - \overrightarrow{r}_p^*\right|^2}{Kn_D^2}, \frac{\left|\overrightarrow{r}_i^* - \overrightarrow{r}_p^*\right|^2}{|\Psi_E| Kn_D^2}\right) \tag{28b}$$

The ion trajectory in free space is approximated accurately by an LD simulation in the limit of $L^* \to \infty$, chosen using eq. (28a) to balance computational expense and accuracy. The selection of $L^* \geq 4000,\ T^* \leq 0.005$ proved adequate to ensure that $\frac{\partial H}{\partial L^*} \approx 0, \frac{\partial H}{\partial T^*} \approx 0$. In the simulation, T^* is used along with eq. (28b) to calculate a variable timestep for each iteration, taking advantage of the linearity between the mean squared displacement and the timestep when the particle and ion are far away from each other and the electrostatic force is small. A related caution is to ensure that the chosen Δt^* results in a positive definite value for $\overrightarrow{R}_r^* \cdot \overrightarrow{R}_r^*$ given by eq. (25d) to ensure a real-valued square root of $\overrightarrow{R}_r^* \cdot \overrightarrow{R}_r^{*\,\frac{1}{2}}$ used in eq. (25c). In practice, Δt^* may be arbitrary reduced until $\overrightarrow{R}_r^* \cdot \overrightarrow{R}_r^* \geq 0$.

Chahl and Gopalakrishnan (2019) describe the H or non-dimensional β_{pi} model development for $0 < \Psi_E \leq 60,\ 0 < Kn_D \leq 2000$ and discuss further aspects of particle charging in aerosols and dusty plasmas. The predictions of LD-based models for β_{pi} including the combined Coulomb and image potential interactions between a spherical particle and ion (Chahl & Gopalakrishnan, 2019; Gopalakrishnan & Hogan, 2012; Li et al., 2020) and a non-spherical particle and ion (Gopalakrishnan, Thajudeen, et al., 2013; Li & Gopalakrishnan, 2021) have been recently compared to available experimental data and have been shown to be accurate to describe diffusion charging of sub-micron, electrically conducting aerosol particles of arbitrary shape in the absence of electric or flow fields (Li et al., 2020; Li & Gopalakrishnan, 2021). As an alternate paradigm to describe diffusion charging of particles without invoking a β_{pi}, LD has been used to describe particle charge fluctuations in aerosols (Gopalakrishnan, Meredith, et al., 2013) and dusty plasmas (Vaulina et al., 2006) that are well corroborated by experimental measurements (Gopalakrishnan et al., 2015a).

Lastly, the first order EB method (eq. (22)) was used to integrate eq. (21) to derive a model for H. Alternately, one may choose to use the fourth order RK method (eq. (17)) as well for the same purpose and the foregoing discussion applies there as well. Without restating the steps of scaling eq. (17) to solve eq. (21), we present calculations of $H(0.01 \leq Kn_D \leq 2000,\ \Psi_E = 30)$ Using both the methods in Fig. 3a. Chahl and Gopalakrishnan (2019) used the EB method for $0.01 \leq Kn_D \leq 2000$, while here we used the EB method for $0.01 \leq Kn_D \leq 200$ and the RK method for $10 \leq Kn_D \leq 2000$, with both methods being used in the range of $10 \leq Kn_D \leq 200$. Also shown, for comparison, are the predictions of the $H(Kn_D,\ \Psi_E)$ put forward by Chahl and Gopalakrishnan (2019) by parameterized H Calculations using the EB method:

$$H(Kn_D, \Psi_E) = e^{\mu} H(Kn_D, \Psi_E = 0) \tag{29a}$$

$$\mu(Kn_D, \Psi_E) = \frac{C}{A}\left(1 + k\frac{\log Kn_D - B}{A}\right)^{-\frac{1}{k}-1} \exp\left(-\left(1 + k\frac{\log Kn_D - B}{A}\right)^{-\frac{1}{k}}\right),\ k \neq 0 \tag{29b}$$

$$H(Kn_D, \Psi_E = 0) = \frac{4\pi Kn_D^2 + 25.836 Kn_D^3 + \sqrt{8\pi} Kn_D\left(11.211 Kn_D^3\right)}{1 + 3.502 Kn_D + 7.211 Kn_D^2 + 11.211 Kn_D^3} \tag{29c}$$

While it is evident that the H calculations derived using both the numerical methods agree within ±10% (Fig. 3b presents $\left(1 - \frac{H_{RK}}{H_{EB}}\right)$% as a function of Kn_D), it is noted that the EB method by virtue of being first order is most accurate and least expensive for $Kn_D < 100$ and the same is true for the RK method for $Kn_D > 10$. Thus, we recommend these methods, respectively, for low-to-transition and transition-to-high Kn_D regimes. Finally, in the range of $10 \leq Kn_D \leq 200$, H Derived using the EB and RK methods are statistically indistinguishable and that the comparisons with experimental data mentioned before apply to simulation results derived using both the numerical schemes. The SI includes Fortran® (.f) implementations of the 3D EB method ("EB_3D_H.f") and 3D RK method ("RK_3D_H.f") for simulating this example with comments.

3.2. Modeling of particle-particle coagulation rate constant in dense aerosols

Coagulation involves collisions between particles that results in particle size growth by sticking and coalescence (in case of easily deformable particles such as liquid droplets). We consider aerosol particle coagulation driven by Brownian motion and hydrodynamic

interactions between particles and the gas medium (drag). Coagulation is the primary driver of particle size distribution changes in ambient or laboratory aerosols and modeling Brownian coagulation in aerosols and dusty plasmas has considerable attention in the past (Chatterjee et al., 1975; Davies, 1979; Fuchs & Sutugin, 1965; Galli & Kortshagen, 2010; Goudeli et al., 2016; Huang et al., 1991; Huang & Seinfeld, 1990; Kortshagen & Bhandarkar, 1999; Kruis et al., 2000; Loyalka, 1976; Lushnikov & Smirnov, 1975a, 1975b; Matsoukas, 1997; Narsimhan & Ruckenstein, 1985a, 1985b; Nowakowski & Sitarski, 1981; Otto & Fissan, 1999; Ravi & Girshick, 2009; Sceats, 1986; Schweigert & Schweigert, 1996; Sitarski & Seinfeld, 1977; Sorensen et al., 1987; Veshchunov & Azarov, 2012; Wagner & Kerker, 1977), including the use of LD for the same (Buesser et al., 2009; Gopalakrishnan et al., 2011; Gopalakrishnan & Hogan, 2011; Heine & Pratsinis, 2007; Hunt et al., 2014; Matthews et al., 2012; Thajudeen et al., 2012, 2014, 2015a; Trzeciak et al., 2004). In line with the scope of this demonstration, we provide just enough details about the physical process itself to follow the computational methodology and refer the interested reader to Gopalakrishnan and Hogan (2011) for a detailed account of model development for the coagulation of *dilute* aerosols ($\eta_v \to 0$) Using LD. The methodology described herein are applied to unravel the coagulation of *dense* aerosols ($0 < \eta_v < 0.1$) as part of an ongoing investigation in the authors' research group (Liu et al., 2020). Recently, Morán, Yon, and Poux (2020); Morán, Yon, Poux, et al. (2020) have incorporated LD-derived timestep into Monte Carlo simulations of particle agglomeration and coagulation-driven growth in dense environments. Similarly, Boies et al. (2019) state that the coagulation rate constant, calculated using LD and experimentally tested, is 1.3–10 times higher for carbon nanotubes than corresponding spheres and is seen as driving the coagulation of highly non-spherical carbon nanotubes into bundles by Brownian motion.

Similar to diffusion charging or broadly, single particle mass transfer processes, the particle-particle collision rate R_{ij} that results in the particle volume being increased from $\vartheta_i \to \vartheta_i + \vartheta_j$, where ϑ_i, ϑ_j are the volumes of the colliding particles (i,j), may be calculated as $R_{ij} = \beta_{ij} n_i n_j$; here, n_i, n_j is the number concentration of particles of kind (i,j).Departing from prior work (Gopalakrishnan & Hogan, 2011), in which particle coagulation was considered as binary particle-particle collision events in the presence of a background gas, we set up a system of N LD ODEs to investigate the coagulation of mono-sized particles at non-trivial volume fractions in a periodic domain:

$$i = 1,\ 2, \ldots N:\ m_i \frac{d\vec{v}_i}{dt} = \vec{F}_D + \vec{F}_B \tag{30}$$

The particle-particle hydrodynamic interactions $\vec{F}_D$ are calculated using Corson's extended Kirkwood-Risemann methodology as described in Section 2.3. For simplicity, we do not include particle-particle adhesion forces, electrostatic effects, fluid flows and external fields in our demonstration and lastly, we ignore particle bounce and assume that particles stick immediately upon collision. The particle-particle diffusive Knudsen number $Kn_D = \frac{\sqrt{m_{ij} k_B T_g}}{f_{ij} a_{ij}}$ that parameterizes the mass transfer regime, the particle momentum Knudsen number $Kn = \frac{\lambda_g}{a_p}$ that describes the momentum transfer regime onto an individual particle and the particle volume fraction $\eta_v = a_p^3 n_p$ determine H, the non-dimensional form of β_{ij}. The sum of particle radii $a_{ij} = a_i + a_j$ is used as the reference length scale, $\frac{m_{ij}}{f_{ij}}$ is the unit of time where $m_{ij} = \frac{m_i m_j}{m_i + m_j}$, $f_{ij} = \frac{f_i f_j}{f_i + f_j}$ and $\frac{a_p f_{ij}}{m_{ij}}$ is a reference particle velocity: in this specific example, we consider only identical particles of radius $a_p = a_i = a_j$; f_p is the single particle scalar friction factor given by eq. (5a). Eq. (30) may be integrated using the EB method (eq. (14)) by rewriting $\vec{F}_D$ as the sum of a single particle drag force $-f_p \vec{v}_i$ and a perturbation term $\delta\vec{F}_D$ that depends on the volume fraction η_v and Kn.

$$\vec{F}_D = -f_p \vec{v}_i + \delta\vec{F}_D(\eta_v, Kn) \tag{31a}$$

$$\delta\vec{F}_D(\eta_v \to 0, Kn) \to 0 \tag{31b}$$

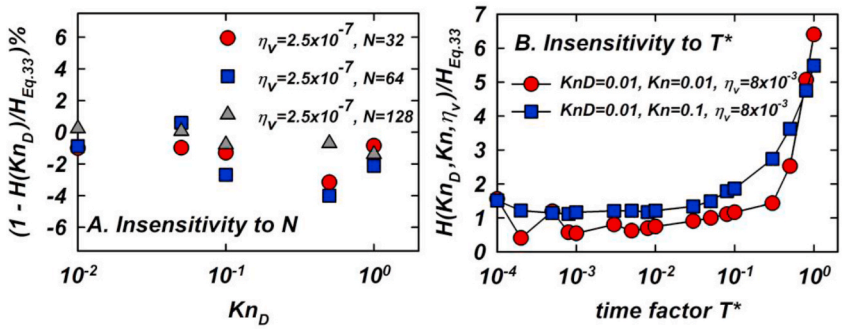

Fig. 4. A. H Calculations in the dilute limit ($\eta_v \to 0$) Compared to the predictions of dilute coagulation model developed by Gopalakrishnan and Hogan (2011) given by eq. (33) using $N = 32,\ 64,\ 128$ Particles in the simulation domain. It is seen that $H(Kn_D, \eta_v \to 0)$ is insensitive to the choice of N. **B.** $H(Kn_D, Kn, \eta_v)$ calculations with $N = 128$ including Kn-dependent hydrodynamic interactions as a function of T^* to determine a suitable value that leads to the simulation results being independent of T^*.

$$i = 1,\ 2, \ldots N:\ m_i \frac{d\vec{v}_i}{dt} = -f_p \vec{v}_i + \delta \vec{F}_D(\eta_v, Kn) + \vec{F}_B \tag{31c}$$

By dynamically simulating a system of N spheres using eq. (31) in a non-dimensional form, the details of which we skip, particle trajectories are analyzed to detect collisions between any particle pair (i,j) Of the N spheres in a periodic domain of side L^*, when $\left|\vec{r}_i^{\,*} - \vec{r}_j^{\,*}\right| \leq 1$, to calculate H as:

$$\frac{\beta_{ij} m_{ij}}{f_{ij} a_p^3} \equiv H = H(Kn_D, Kn,\ \eta_v) = \frac{L^{*3}}{\tau^*} \frac{1}{C(N,2)} \tag{32a}$$

$$\tau^* = \frac{1}{N_T} \sum_{k=1}^{N_T} \tau_k \tag{32b}$$

τ^* is the mean particle-particle collision time averaged over N_T~2000 collisions of an ergodic simulation. $C(N,r) = \frac{N!}{(N-r)!r!}$ is included to account for collision between any pair of N identical particles. Eq. (32) may be derived as follows: $\beta_{ij} = \frac{R_{ij}}{n_i n_j}$. R_{ij} is the number of collisions per unit volume per unit time and may be evaluated from LD simulations as $R_{ij} = \frac{1}{\tau}\frac{1}{L^3}$ and $n_i = n_j = \frac{N}{L^3}$, leading to $\beta_{ij} = \frac{L^3}{\tau}\frac{1}{C(N,2)}$; L is the simulation box side, τ is the dimensional particle-particle collision time over N_T collisions. This equation is expressed in non-dimensional form in Eq. (32). The ergodicity of this equation was checked by simulating cases of dilute or low-volume fraction aerosols as shown in Fig. 4a that shows that the derived H values are independent of N as $\eta_v \to 0$. When two particles collide, they are initialized with a newly sampled position in the simulation box (while checking that the new position does not overlap with other particles) and velocity from the Maxwell-Boltzmann distribution, similar to the case of ion trajectory simulations in Section 3.1. H estimated using eq. (32) is compared with $H(Kn_D,\ \eta_v \to 0)$ derived previously by Gopalakrishnan and Hogan (2011) in the limit of $\eta_v \to 0$ as a consistency check (same as eq. (29c)):

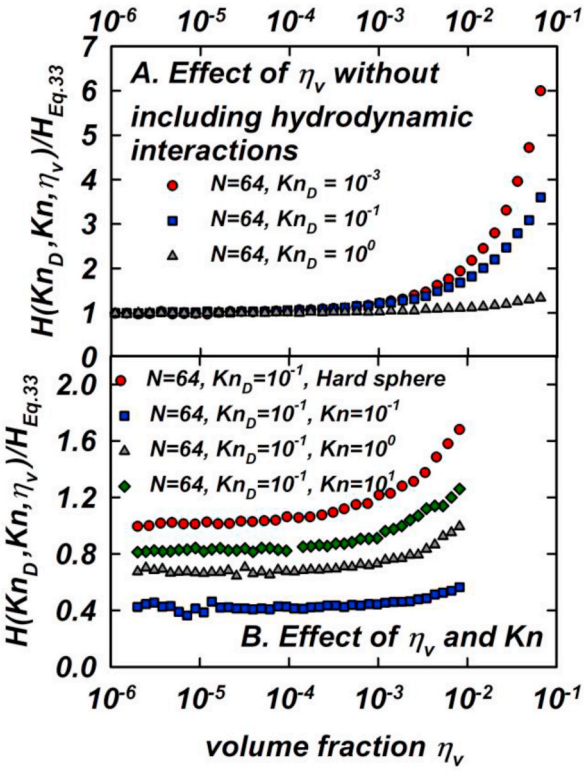

Fig. 5. A. $H(Kn_D, Kn, \eta_v)$ calculations to probe the effect of volume fraction $0 < \eta_v < 10^{-1}$ without including hydrodynamic interactions (no Kn Dependence) that shows the enhancement compared to the predictions of dilute coagulation rate constant model (eq. (33)). **B.** $H(Kn_D, Kn, \eta_v)$ calculations to probe the combined effect of volume fraction $0 < \eta_v < 10^{-2}$ and Kn-dependent hydrodynamic interactions.

$$H(Kn_D, \eta_v \to 0) = \frac{4\pi Kn_D^2 + 25.836 Kn_D^3 + \sqrt{8\pi} Kn_D \left(11.211 Kn_D^3\right)}{1 + 3.502 Kn_D + 7.211 Kn_D^2 + 11.211 Kn_D^3} \tag{33}$$

L^* is selected using the target volume fraction η_v and N:

$$L^* = \left(\frac{\pi}{6}\frac{N}{\eta_v}\right)^{\frac{1}{3}} \tag{34a}$$

Fig. 4a presents $\left(1 - \frac{H_N}{H_{Eq.33}}\right)\%$ for $0.01 \le Kn_D \le 100, \eta_v = 2.5 \times 10^{-7}$ while varying $N = 32, 64, 128$ particles. It is seen that H_N, H calculated by simulating N particles in a periodic domain of volume L^{*3}, is independent of N, showing that the simulation predictions in the $\eta_v \to 0$ limit are in line with prior work (eq. (33)). The timestep Δt^* is chosen by comparing the displacement step due to hydrodynamic force and diffusion:

$$\Delta t^* = T^* \min\left(\frac{1}{\left|\delta \vec{F}_D^{\,*}\right|^{max}}, \frac{\left|\vec{r}_{ij}^{\,*}\right|^{min}}{Kn_D^2}\right) \tag{34b}$$

Here, $\left|\delta \vec{F}_D^{\,*}\right|^{max}$ is the maximum of hydrodynamic force perturbation $\delta \vec{F}_{D,i}$ experienced by $i = 1 - N$ particles and $\left|\vec{r}_{ij}^{\,*}\right|^{min}$ is the minimum of particle pairwise seperations for all pairs $1 \le i \le N, 1 \le j \ne i \le N$. Fig. 4b presents $H(Kn_D,\ Kn, \eta_v)$ as a function of T^* that shows that a selection of $T^* \le 0.005$ sufficiently mitigates any influence of timestep on trajectory simulations for H calculations. In general, T^* must be chosen to establish $\frac{\partial H}{\partial T^*} \approx 0$. Fig. 5a present preliminary results of the calculation of $\beta_r = \frac{H(Kn_D, \eta_v)}{H_{Eq.33}}$ as a function of η_v for $Kn_D = 0.001, 0.1, 1.0$, *without* including hydrodynamic interactions $(\delta \vec{F}_D(\eta_v, Kn) = 0)$ to understand the effect of particle volume fraction on coagulation. It is seen that β_r is *enhanced* by ~2–6 times for $\eta_v > 10^{-2}$. Similarly, Fig. 5b plots $\beta_r = \frac{H(Kn_D, Kn, \eta_v)}{H_{Eq.33}}$ while including both the effects of η_v and Kn-dependent hydrodynamic interactions $\delta \vec{F}_D(\eta_v, Kn)$. In this case, it is seen that there is a *reduction* by ~1–2.5 times that is dependent on Kn at a fixed $Kn_D = 0.1$. Hard sphere interactions $(Kn \to \infty)$ represents the limit of vanishing hydrodynamic interactions, that become more significant with decreasing Kn up to 0.1. A more detailed study of the coagulation of dense aerosols is currently underway (Liu et al., 2020) and the computational results obtained therein will need to compared with prior theories on the coagulation of dense aerosols (Veshchunov & Tarasov, 2014).

4. Summary

We have demonstrated the usage of LD for simulating particle trajectories and to derive collision rate constants by averaging over an ensemble of simulated trajectories. We have described the considerations for selecting simulation parameters such as domain size and time step in an LD simulation that is usually omitted from regular articles that are focused on aerosol physics. We have also provided Fortran® and MATLAB® computer codes with comments for the benefit of the interested reader. The following remarks are in order to conclude this tutorial:

1. Although, not discussed in detail in this tutorial, LD has been used numerously in the field of dusty plasmas as well to extract transport and thermodynamic properties of electrostatically coupled charged dust grains suspended in a partially ionized gas at low pressures (<500 Pa): dust particle pair correlation and bond order functions (Petrov et al., 2005; Ratynskaia et al., 2009; Smith et al., 2004; Vaulina, 2009; Vaulina & Dranzhevskii, 2007; Vaulina et al., 2004, 2007, 2011; Vaulina & Petrov, 2004), as well as dusty particle phase transport coefficients such as self-diffusion coefficient (Khrapak et al., 2012; Liu & Goree, 2007, 2014, 2016b; Vaulina & Dranzhevskii, 2007), shear viscosity (Donkó et al., 2006; Donko et al., 2009; Feng et al., 2011, 2012, 2013; Haralson & Goree, 2017; Liu & Goree, 2005, 2016a; Nosenko & Goree, 2004), shear modulus (Liu & Goree, 2017) and dust particle thermodynamic equations of state in the authors' current work (Gopalakrishnan et al., 2020; Suresh et al., 2020)
2. LD is also widely used to model particle motion in flow devices for design and evaluation as well. Examples include: Liu et al. (Liu et al., 1995a, 1995b) and Wang et al. (Wang et al., 2005a, 2005b) used LD to track particles along with gas flow at low pressure for designing aerodynamic lenses for particle focusing. The fluid flow field obtained using CFD was one-way coupled to the equations of particle motion for calculating the resulting trajectories. Nikbakht et al. (2006) and Abouali et al. (2009) similarly use LD to track the 3D motion of particles for optimizing the design of aerodynamic lenses for minimizing particle Brownian motion. Recently, Ahmed and Gopalakrishnan (2019) used LD (with and without including the stochastic force term $\vec{F}_B(t)$) to analyze the electrostatic focusing of aerosol particles using a 3-electrode Einzel lens. Dubey and Dhaniyala (2011) use LD to estimate the diffusional transfer function of differential mobility analyzers by coupling particle motion to an axisymmetric flow field. Likewise, Oberreit et al. (2014) use LD to calculate particle arrival time distributions in a drift tube aerosol mobility spectrometer to develop instrument response/transfer function.

3. While LD has many potential applications to simulate aerosol particle motion in the finite Kn_D transition regime, the limitations of the same must also be kept in mind while selecting a trajectory simulation technique for a specific application. Thermal equilibrium between the suspended particles and the background gas molecules is a pre-requisite to apply LD modeling; thus, modeling particle transport in conditions far from equilibrium ($Kn \to \infty,\ t_s > t_r$) must be approached with caution. Another assumption built into the LD formalism is that the suspended particle is much heavier than the background gas molecules ($m_p \gg m_g$); m_p is particle mass and m_g is the mass of a background gas molecule. Aerosol particles that are >2 nm and macromolecules that are at least a few ~100 Da satisfy this requirement in most background gases. The simulation of atomic or light ions for which $m_p \tilde{} m_g$ using LD requires a fundamental reexamination of the formulation of eq. (1) that is currently not known, as they represent a lower limit to the size/mass of particles that are amenable to an LD description through the use of continuum approximations for the particle-gas interactions. Lastly, although not discussed in this tutorial, consideration of particle rotation and the translation-rotation coupling is a considerably more complex endeavor than simulating pure translational motion discussed here – the rotational Langevin equations for a single particle needs to be solved in a frame of reference that is attached to and rotates at the same angular rate as the particle. This precludes the description of a system of particles in a common laboratory frame of reference. Also, a quaternion-based rotational degrees of freedom is necessary to describe the evolution of the orientation and angular rate of rotation of a particle (Davidchack et al., 2017) instead of the use of Eulerian angles that is applicable only for particles with special symmetries (Berkowitz et al., 1983; Dickinson et al., 1985a, 1985b; Huber & McCammon, 2010; Northrup et al., 1984, 1986).
4. Lastly, a disadvantage of LD simulations is the high CPU time, especially when simulating systems consisting of a large number of interacting particles. Implementational issues devoted to optimizing the CPU time, such as implementing linked-cell methods, neighbor lists, ghost domains when simulating coagulation of dense aerosols, periodic boundary conditions and few other aspects of N-particle simulations such as the truncation of interaction potentials at long particle-particle separations were not discussed in this tutorial as these issues have been well developed in the context of MD simulations (Allen & Tildesley, 1991; Bird, 1994) and LD simulations (Huber & McCammon, 2010). While selecting a computational technique, it is important that one balances the level of detail required in particle position and velocity timeseries to the computational expense and utility in obtaining the same. In the limit of a large number of interacting particles, in principle, a Lagrangian tracking approach such as LD would approach a field description of the collective transport of particles that provides less information about individual particles but also comes with a modest computational expense.

About the article

This article is an Editor-Invited Tutorial Article. Tutorial Articles, established to commemorate the 50th Anniversary of the Journal of Aerosol Science in 2020, are intended to serve as educational resources for the aerosol research community on state-of-the-art experimental, theoretical, and numerical techniques in aerosol science.

Declaration of competing interest

The authors declare that they have no known competing financial interests or personal relationships that could have appeared to influence the work reported in this paper.

Acknowledgements

Funding for this work was provided by US National Science Foundation (NSF) PHY Grant Award Number 1903432 under the Directorate of Mathematical & Physical Sciences, US Department of Energy Office of Science Grant Award Number DE-SC0021146 from the Office of Fusion Energy Sciences and Grant Award Number DE-SC0021206 from the Office of Basic Energy Sciences. We thank the University of Memphis High Performance Computing Cluster for providing computational resources to carry out this research. The authors thank Mr. Harjindar Chahl, Mr. Zhibo Liu and Ms. Li Li for helpful discussions on this topic. R. G. thanks Prof. Chris Hogan for many insightful discussions about aerosol physics over the years.

Appendix A. Supplementary data

Supplementary data to this article can be found online at https://doi.org/10.1016/j.jaerosci.2021.105746.

References

Abouali, O., Nikbakht, A., Ahmadi, G., & Saadabadi, S. (2009). Three-dimensional simulation of brownian motion of nano-particles in aerodynamic lenses. *Aerosol Science and Technology, 43*(3), 205–215. https://doi.org/10.1080/02786820802587888

Ahmed, R., & Gopalakrishnan, R. (2019). Computational study of electrostatic focusing of aerosol nanoparticles using an einzel lens. *Journal of Aerosol Science, 137*, 105443. https://doi.org/10.1016/j.jaerosci.2019.105443

Albers, J., Deutch, J. M., & Oppenheim, I. (1971). Generalized Langevin equations. *The Journal of Chemical Physics, 54*(8), 3541–3546. https://doi.org/10.1063/1.1675378

Allen, M. P., & Tildesley, D. J. (1991). *Computer simulation of liquids*. Oxford: Clarendon Press.

Bardsley, J. N., & Wadehara, J. M. (1980). Monte Carlo simulation of three-body ion-ion recombination. *Chemical Physics Letters, 72*(3), 477–480. https://doi.org/10.1016/0009-2614(80)80335-6
Berkowitz, M., Morgan, J. D., & McCammon, J. A. (1983). Generalized Langevin dynamics simulations with arbitrary time-dependent memory kernels. *The Journal of Chemical Physics, 78*(6), 3256–3261. https://doi.org/10.1063/1.445244
Bird, G. A. (1994). *Molecular gas dynamics and the direct simulation of gas flows*. Oxford: Clarendon.
Boies, A. M., Hoecker, C., Bhalerao, A., Kateris, N., de La Verpilliere, J., Graves, B., & Smail, F. (2019). Agglomeration dynamics of 1d materials: Gas-phase collision rates of nanotubes and nanorods. *Small, 15*(27), 1900520. https://doi.org/10.1002/smll.201900520, 10.1002/smll.201900520.
Brady, J. F., & Bossis, G. (1988). Stokesian dynamics. *Annual Review of Fluid Mechanics, 20*(1), 111–157. https://doi.org/10.1146/annurev.fl.20.010188.000551
Brady, J. F., Phillips, R. J., Lester, J. C., & Bossis, G. (1988). Dynamic simulation of hydrodynamically interacting suspensions. *Journal of Fluid Mechanics, 195*, 257–280. https://doi.org/10.1017/S0022112088002411
Brady, J. F., & Sierou, A. (2001). Accelerated stokesian dynamics simulations. *Journal of Fluid Mechanics, 448*, 115–146.
Brenner, H. (1963). The Stokes resistance of an arbitrary particle. *Chemical Engineering Science, 18*(1), 1–25. https://doi.org/10.1016/0009-2509(63)80001-9
Brenner, H. (1964). The Stokes resistance of an arbitrary particle—ii. *Chemical Engineering Science, 19*(9), 599–629. https://doi.org/10.1016/0009-2509(64)85051-X
Brenner, H. (1965). Coupling between the translational and rotational brownian motions of rigid particles of arbitrary shape i. Helicoidally isotropic particles. *Journal of Colloid Science, 20*(2), 104–122. https://doi.org/10.1016/0095-8522(65)90002-4
Brenner, H. (1967). Coupling between the translational and rotational brownian motions of rigid particles of arbitrary shape: Ii. General theory. *Journal of Colloid and Interface Science, 23*(3), 407–436. https://doi.org/10.1016/0021-9797(67)90185-3
Bricard, J. (1962). La fixation des petits ions atmosphériques sur les aérosols ultra-fins. *Geofisica pura e applicata, 51*(1), 237–242. https://doi.org/10.1007/BF01992666
Buesser, B., Heine, M. C., & Pratsinis, S. E. (2009). Coagulation of highly concentrated aerosols. *Journal of Aerosol Science, 40*(2), 89–100. https://doi.org/10.1016/j.jaerosci.2008.09.005
Chahl, H. S., & Gopalakrishnan, R. (2019). High potential, near free molecular regime coulombic collisions in aerosols and dusty plasmas. *Aerosol Science and Technology, 53*(8), 933–957. https://doi.org/10.1080/02786826.2019.1614522
Chandrasekhar, S. (1943). Stochastic problems in physics and astronomy. *Reviews of Modern Physics, 15*(1), 1–89. https://doi.org/10.1103/RevModPhys.15.1
Chapman, S., & Cowling, T. G. (1991). *The mathematical theory of non-uniform gases*. Cambridge, UK: Cambridge University Press.
Chatterjee, A., Kerker, M., & Cooke, D. D. (1975). Brownian coagulation of aerosols in the transition regime. *Journal of Colloid and Interface Science, 53*, 71–82.
Chen, Z. Y., Deutch, J. M., & Meakin, P. (1984). Translational friction coefficient of diffusion limited aggregates. *The Journal of Chemical Physics, 80*(6), 2982–2983. https://doi.org/10.1063/1.447012
Coffey, W. T., Kalmykov, Y. P., & Waldron, J. T. (2004). *The Langevin equation* (Vol. 14). WORLD SCIENTIFIC.
Collins, D. R., Smith, W., Harrison, N. M., & Forester, T. R. (1996). Molecular dynamics study of tio 2 microclusters. [10.1039/JM9960601385]. *Journal of Materials Chemistry, 6*(8), 1385–1390. https://doi.org/10.1039/JM9960601385
Coots, J., Gandhi, V., Onakoya, T., Chen, X., & Larriba-Andaluz, C. (2020). A parallelized tool to calculate the electrical mobility of charged aerosol nanoparticles and ions in the gas phase. *Journal of Aerosol Science, 147*, 105570. https://doi.org/10.1016/j.jaerosci.2020.105570
Corson, J. (2018). *Predicting the transport properties of aerosol particles in creeping flow from the continuum to the free molecule regime*. Ph. D. College Park: University of Maryland
Corson, J., Mulholland, G. W., & Zachariah, M. R. (2017a). Analytical expression for the friction coefficient of dlca aggregates based on extended kirkwood-riseman theory. *Aerosol Science and Technology, 51*(6), 766–777. https://doi.org/10.1080/02786826.2017.1300635
Corson, J., Mulholland, G. W., & Zachariah, M. R. (2017b). Calculating the rotational friction coefficient of fractal aerosol particles in the transition regime using extended kirkwood-riseman theory. *Physical Review E, 96*(1), Article 013110.
Corson, J., Mulholland, G. W., & Zachariah, M. R. (2017c). Friction factor for aerosol fractal aggregates over the entire knudsen range. *Physical Review E, 95*(1). https://doi.org/10.1103/PhysRevE.95.013103
Corson, J., Mulholland, G. W., & Zachariah, M. R. (2018a). Analytical expression for the rotational friction coefficient of dlca aggregates over the entire knudsen regime. *Aerosol Science and Technology, 52*(2), 209–221. https://doi.org/10.1080/02786826.2017.1390544
Corson, J., Mulholland, G. W., & Zachariah, M. R. (2018b). Hydrodynamic interactions between aerosol particles in the transition regime. *Journal of Fluid Mechanics, 855*, 535–553. https://doi.org/10.1017/jfm.2018.632
Cunningham, E. (1910). On the velocity of steady fall of spherical particles through fluid medium. *Proceedings of the Royal Society of London. Series A., 83*(563), 357–365.
D'Yachkov, L. G., Khrapak, A. G., Khrapak, S. A., & Morfill, G. (2007). Model of grain charging in collisional plasmas accounting for collisionless layer. *Physics of Plasmas, 14*.
Dahneke, B. E. (1973a). Slip correction factors for nonspherical bodies- i introduction and continuum flow. *Journal of Aerosol Science, 4*, 139–145.
Dahneke, B. E. (1973b). Slip correction factors for nonspherical bodies- ii free molecular flow. *Journal of Aerosol Science, 4*, 147–161.
Dahneke, B. E. (1973c). Slip correction factors for nonspherical bodies- iii the form of the general law. *Journal of Aerosol Science, 4*, 163–170.
Daneshian, B., & Assadi, H. (2014). Impact behavior of intrinsically brittle nanoparticles: A molecular dynamics perspective. *Journal of Thermal Spray Technology, 23*(3), 541–550. https://doi.org/10.1007/s11666-013-0019-4
Davidchack, R. L., Handel, R., & Tretyakov, M. V. (2009). Langevin thermostat for rigid body dynamics. *The Journal of Chemical Physics, 130*(23), 234101. https://doi.org/10.1063/1.3149788
Davidchack, R. L., Ouldridge, T. E., & Tretyakov, M. V. (2017). Geometric integrator for Langevin systems with quaternion-based rotational degrees of freedom and hydrodynamic interactions. *The Journal of Chemical Physics, 147*(22), 224103. https://doi.org/10.1063/1.4999771
Davies, C. N. (1945). Definitive equations for the fluid resistance of spheres. *Proceedings of the Physical Society, 57*, 259–270.
Davies, C. N. (1979). Coagulation of aerosols by brownian-motion. *Journal of Aerosol Science, 10*(2), 151–161. https://doi.org/10.1016/0021-8502(79)90064-8
Dawes, J. M., & Sceats, M. G. (1988). Biomolecular reactions on surfaces. Theory for arbitrary mean free path. *The Journal of Chemical Physics, 88*, 5489–5495.
Delong, S., Usabiaga, F. B., & Donev, A. (2015). Brownian dynamics of confined rigid bodies. [Article]. *The Journal of Chemical Physics, 143*(14), 24. https://doi.org/10.1063/1.4932062
Deutch, J. M., & Oppenheim, I. (1971). Molecular theory of brownian motion for several particles. *The Journal of Chemical Physics, 54*(8), 3547–3555. https://doi.org/10.1063/1.1675379
Dhaubhadel, R., Chakrabarti, A., & Sorensen, C. M. (2009). Light scattering study of aggregation kinetics in dense, gelling aerosols. *Aerosol Science and Technology, 43*(11), 1053–1063. https://doi.org/10.1080/02786820903136908
Dhaubhadel, R., Rieker, T. P., Chakrabarti, A., & Sorensen, C. M. (2012). Synthesis of silica aerosol gels via controlled detonation. *Aerosol Science and Technology, 46*(5), 596–600. https://doi.org/10.1080/02786826.2011.651175
Dickinson, E., Allison, S. A., & McCammon, J. A. (1985a). Brownian dynamics with rotation-translation coupling. [10.1039/F29858100591]. *Journal of the Chemical Society, Faraday Transactions 2: Molecular and Chemical Physics, 81*(4), 591–601. https://doi.org/10.1039/F29858100591
Dickinson, E., Allison, S. A., & McCammon, J. A. (1985b). Brownian dynamics with rotation–translation coupling. [10.1039/F29858100591]. *Journal of the Chemical Society, Faraday Transactions 2: Molecular and Chemical Physics, 81*(4), 591–601. https://doi.org/10.1039/F29858100591
Dong, Y., Vadakkepatt, A., & Martini, A. (2011). Analytical models for atomic friction. *Tribology Letters, 44*(3), 367. https://doi.org/10.1007/s11249-011-9850-2
Donkó, Z., Goree, J., Hartmann, P., & Kutasi, K. (2006). Shear viscosity and shear thinning in two-dimensional yukawa liquids. *Physical Review Letters, 96*(14), 145003. https://doi.org/10.1103/PhysRevLett.96.145003
Donko, Z., Goree, J., Hartmann, P., & Liu, B. (2009). Time-correlation functions and transport coefficients of two-dimensional yukawa liquids. *Physical Review E, 79*(2). https://doi.org/10.1103/PhysRevE.79.026401

Douglas, J. F., Zhou, H. X., & Hubbard, J. B. (1994). Hydrodynamic friction and the capacitance of arbitrarily-shaped objects. [Article]. *Physical Review E, 49*(6), 5319–5337.

Dubey, P., & Dhaniyala, S. (2011). A new approach to calculate diffusional transfer functions of scanning dmas. *Aerosol Science and Technology, 45*(8), 1031–1040. https://doi.org/10.1080/02786826.2011.579644. doi: 10.1080/02786826.2011.579644.

Epstein, P. S. (1924). On the resistance experienced by spheres in their motion through gases. *Physical Review, 23*(6), 710–733.

Ermak, D. L., & Buckholz, H. (1980). Numerical integration of the Langevin equation: Monte Carlo simulation. *Journal of Computational Physics, 35*(2), 169–182. https://doi.org/10.1016/0021-9991(80)90084-4

Feng, Y., Goree, J., & Liu, B. (2011). Viscosity calculated in simulations of strongly coupled dusty plasmas with gas friction. *Physics of Plasmas, 18*(5). https://doi.org/10.1063/1.3560584

Feng, Y., Goree, J., & Liu, B. (2012). Energy transport in a shear flow of particles in a two-dimensional dusty plasma. *Physical Review E, 86*(5). https://doi.org/10.1103/PhysRevE.86.056403

Feng, Y., Goree, J., & Liu, B. (2013). Longitudinal viscosity of two-dimensional yukawa liquids. *Physical Review E, 87*(1). https://doi.org/10.1103/PhysRevE.87.013106

Friedlander, S. K. (2000). *Smoke, dust, and haze*. New York: Oxford University Press.

Fuchs, N. A. (1963). On the stationary charge distribution on aerosol particles in a bipolar ionic atmosphere. *Geofis. Pura Appl., 51*, 185–193.

Fuchs, N. A., & Sutugin, A. G. (1965). Coagulation rate of highly dispersed aerosols. *Journal of Colloid Science, 20*, 492–500.

Galli, F., & Kortshagen, U. R. (2010). Charging, coagulation, and heating model of nanoparticles in a low-pressure plasma accounting for ion-neutral collisions. *IEEE Transactions on Plasma Science, 38*(4), 803–809. https://doi.org/10.1109/tps.2009.2035700

Gatti, M., & Kortshagen, U. (2008). Analytical model of particle charging in plasmas over a wide range of collisionality. [Article]. *Physical Review E, 78*(4), Article 046402. https://doi.org/10.1103/PhysRevE.78.046402

Given, J. A., Hubbard, J. B., & Douglas, J. F. (1997). A first-passage algorithm for the hydrodynamic friction and diffusion-limited reaction rate of macromolecules. *The Journal of Chemical Physics, 106*(9), 3761–3771.

Gopalakrishnan, R., & Hogan, C. J. (2011). Determination of the transition regime collision kernel from mean first passage times. *Aerosol Science and Technology, 45*(12), 1499–1509. https://doi.org/10.1080/02786826.2011.601775

Gopalakrishnan, R., & Hogan, C. J. (2012). Coulomb-influenced collisions in aerosols and dusty plasmas. *Physical Review E, 85*, Article 026410.

Gopalakrishnan, R., McMurry, P. H., & Hogan, C. J. (2015a). The bipolar diffusion charging of nanoparticles: A review and development of approaches for non-spherical particles. *Aerosol Science and Technology, 49*(12), 1181–1194. https://doi.org/10.1080/02786826.2015.1109053

Gopalakrishnan, R., McMurry, P. H., & Hogan, C. J., Jr. (2015b). The electrical mobilities and scalar friction factors of modest-to-high aspect ratio particles in the transition regime. *Journal of Aerosol Science, 82*, 24–39. https://doi.org/10.1016/j.jaerosci.2015.01.001, 0.

Gopalakrishnan, R., Meredith, M. J., Larriba-Andaluz, C., & Hogan, C. J. (2013). Brownian dynamics determination of the bipolar steady state charge distribution on spheres and non-spheres in the transition regime. *Journal of Aerosol Science, 63*, 126–145. https://doi.org/10.1016/j.jaerosci.2013.04.007

Gopalakrishnan, R., Suresh, V., & Liu, Z. (2020). Thermodynamic equations of state for the dust grain using Langevin dynamics simulations. In *Paper presented at the 62nd annual meeting of the APS division of plasma physics, virtual conference*.

Gopalakrishnan, R., Thajudeen, T., & Hogan, C. J. (2011). Collision limited reaction rates for arbitrarily shaped particles across the entire diffusive knudsen number range. *The Journal of Chemical Physics, 135*, Article 054302.

Gopalakrishnan, R., Thajudeen, T., Ouyang, H., & Hogan, C. J. (2013). The unipolar diffusion charging of arbitrary shaped aerosol particles. *Journal of Aerosol Science, 64*, 60–80. https://doi.org/10.1016/j.jaerosci.2013.06.002, 0.

Gordon, D., Hoyles, M., & Chung, S.-H. (2009). Algorithm for rigid-body brownian dynamics. *Physical Review E, 80*(6), Article 066703. https://doi.org/10.1103/PhysRevE.80.066703

Goudeli, E., Eggersdorfer, M. L., & Pratsinis, S. E. (2016). Coagulation of agglomerates consisting of polydisperse primary particles. *Langmuir, 32*(36), 9276–9285. https://doi.org/10.1021/acs.langmuir.6b02455

Goudeli, E., & Pratsinis, S. E. (2016). Gas-phase manufacturing of nanoparticles: Molecular dynamics and mesoscale simulations. *Particulate Science & Technology, 34*(4), 483–493. https://doi.org/10.1080/02726351.2016.1138263

Happel, J., & Brenner, H. (2012). *Low Reynolds number hydrodynamics: With special applications to particulate media*. Netherlands: Springer.

Haralson, Z., & Goree, J. (2017). Overestimation of viscosity by the green-kubo method in a dusty plasma experiment. *Physical Review Letters, 118*(19). https://doi.org/10.1103/PhysRevLett.118.195001

Hawa, T., & Zachariah, M. R. (2007). Development of a phenomenological scaling law for fractal aggregate sintering from molecular dynamics simulation. *Journal of Aerosol Science, 38*(8), 793–806. https://doi.org/10.1016/j.jaerosci.2007.05.008

Heine, M. C., & Pratsinis, S. E. (2007). Brownian coagulation at high concentration. *Langmuir, 23*(19), 9882–9890. https://doi.org/10.1021/la7012599

Hiemenz, P. C., & Rajagopalan, R. (1997). *Principles of colloid and surface chemistry* (3rd ed.). Taylor & Francis. revised and expanded.

Hogan, C. J., & Fernandez de la Mora, J. (2011). Ion mobility measurements of non-denatured 12 - 150 kda proteins and protein multimers by tandem differential mobility analysis - mass spectrometry (dma-ms). *Journal of the American Society for Mass Spectrometry, 22*, 158–172.

Hoppel, W. A., & Frick, G. M. (1986). Ion-aerosol attachment coefficients and the steady-state charge distribution on aerosols in a bipolar ion environment. *Aerosol Science and Technology, 5*(1), 1–21.

Huang, D. D., & Seinfeld, J. H. (1990). Fokker-planck equation solution of aerosol brownian coagulation with an interparticle potential. *Journal of Colloid and Interface Science, 139*(1), 213–237. https://doi.org/10.1016/0021-9797(90)90458-z

Huang, D. D., Seinfeld, J. H., & Okuyama, K. (1991). Image potential between a charged-particle and an uncharged particle in aerosol coagulation enhancement in all size regimes and interplay with vanderwaals forces. *Journal of Colloid and Interface Science, 141*(1), 191–198.

Hubbard, P. S. (1972). Rotational brownian motion. *Physical Review A, 6*(6), 2421–2433. https://doi.org/10.1103/PhysRevA.6.2421

Hubbard, P. S. (1973). Rotational brownian motion. Ii. Fourier transforms for a spherical body with strong interactions. *Physical Review A, 8*(3), 1429–1436. https://doi.org/10.1103/PhysRevA.8.1429

Hubbard, P. S. (1977). Angular velocity of a nonspherical body undergoing rotational brownian motion. *Physical Review A, 15*(1), 329–336. https://doi.org/10.1103/PhysRevA.15.329

Hubbard, J. B., & Douglas, J. F. (1993). Hydrodynamic friction of arbitrarily shaped brownian particles. *Physical Review E, 47*(5), R2983–R2986.

Huber, G. A., & McCammon, J. A. (2010). Browndye: A software package for brownian dynamics. *Computer Physics Communications, 181*(11), 1896–1905. https://doi.org/10.1016/j.cpc.2010.07.022

Hunt, B., Thajudeen, T., & Hogan, C. J. (2014). The single-fiber collision rate and filtration efficiency for nanoparticles i: The first-passage time calculation approach. *Aerosol Science and Technology, 48*(8), 875–885. https://doi.org/10.1080/02786826.2014.938798

Ilie, I. M., Briels, W. J., & den Otter, W. K. (2015). An elementary singularity-free rotational brownian dynamics algorithm for anisotropic particles. *The Journal of Chemical Physics, 142*(11), 114103. https://doi.org/10.1063/1.4914322

Jackson, J. D. (1975). *Classical electrodynamics*. Wiley.

Jeans, J. (1925). *Mathematical theory of electricity and magnetism*. Cambridge: Cambridge University Press.

Kasdin, N. J. (1995). Runge-Kutta algorithm for the numerical integration of stochastic differential equations. *Journal of Guidance, Control, and Dynamics, 18*(1), 114–120. https://doi.org/10.2514/3.56665

Kasdin, N. J., & Stankievech, L. J. (2009). On simulating randomly driven dynamic systems. *Journal of the Astronautical Sciences, 57*(1), 289–311. https://doi.org/10.1007/BF03321506

Khrapak, S. A., Vaulina, O. S., & Morfill, G. E. (2012). Self-diffusion in strongly coupled yukawa systems (complex plasmas). *Physics of Plasmas, 19*(3). https://doi.org/10.1063/1.3691960

Kim, S., & Oppenheim, I. (1972). Molecular theory of brownian motion in external fields. *Physica, 57*(4), 469–482. https://doi.org/10.1016/0031-8914(72)90040-7

Kirkwood, J. G., & Riseman, J. (1948). The intrinsic viscosities and diffusion constants of flexible macromolecules in solution. *The Journal of Chemical Physics, 16*(6), 565–573. https://doi.org/10.1063/1.1746947

Knutson, E. O., & Whitby, K. T. (1975). Aerosol classification by electric mobility: Apparatus, theory, and applications. *Journal of Aerosol Science, 6*(6), 443–451. https://doi.org/10.1016/0021-8502(75)90060-9

Koparde, V. N., & Cummings, P. T. (2008). Sintering of titanium dioxide nanoparticles: A comparison between molecular dynamics and phenomenological modeling. *Journal of Nanoparticle Research, 10*(7), 1169–1182. https://doi.org/10.1007/s11051-007-9342-3

Kortshagen, U., & Bhandarkar, U. (1999). Modeling of particulate coagulation in low pressure plasmas. *Physical Review E, 60*(1), 887–898. https://doi.org/10.1103/PhysRevE.60.887

Kruis, F. E., Maisels, A., & Fissan, H. (2000). Direct simulation Monte Carlo method for particle coagulation and aggregation. *AIChE Journal, 46*(9), 1735–1742. https://doi.org/10.1002/aic.690460905

Ku, B. K., & de la Mora, J. F. (2009). Relation between electrical mobility, mass, and size for nanodrops 1-6.5 nm in diameter in air. *Aerosol Science and Technology, 43*(3), 241–249. https://doi.org/10.1080/02786820802590510

Larriba-Andaluz, C., & Carbone, F. (2021). The size-mobility relationship of ions, aerosols, and other charged particle matter. *Journal of Aerosol Science, 151*, 105659. https://doi.org/10.1016/j.jaerosci.2020.105659

Larriba-Andaluz, C., & Prell, J. S. (2020). Fundamentals of ion mobility in the free molecular regime. Interlacing the past, present and future of ion mobility calculations. *International Reviews in Physical Chemistry, 39*(4), 569–623. https://doi.org/10.1080/0144235X.2020.1826708

Larriba, C., & Fernandez de la Mora, J. (2012). The gas phase structure of coulombically stretched polyethylene glycol ions. *The Journal of Physical Chemistry B, 116*(1), 593–598. https://doi.org/10.1021/jp2092972

Larriba, C., & Hogan, C. J. (2013a). Free molecular collision cross section calculation methods for nanoparticles and complex ions with energy accommodation. *Journal of Computational Physics, 251*, 344–363. https://doi.org/10.1016/j.jcp.2013.05.038

Larriba, C., & Hogan, C. J. (2013b). Ion mobilities in diatomic gases: Measurement versus prediction with non-specular scattering models. *The Journal of Physical Chemistry A, 117*(19), 3887–3901. https://doi.org/10.1021/jp312432z. doi: 10.1021/jp312432z.

Larriba, C., Hogan, C. J., Jr., Attoui, M., Borrajo, R., Garcia, J. F., & de la Mora, J. F. (2011). The mobility-volume relationship below 3.0 nm examined by tandem mobility-mass measurement. *Aerosol Science and Technology, 45*(4), 453–467. https://doi.org/10.1080/02786826.2010.546820

Lazzari, S., Nicoud, L., Jaquet, B., Lattuada, M., & Morbidelli, M. (2016). Fractal-like structures in colloid science. *Advances in Colloid and Interface Science, 235*, 1–13. https://doi.org/10.1016/j.cis.2016.05.002

Li, L., Chahl, H. S., & Gopalakrishnan, R. (2020). Comparison of the predictions of Langevin dynamics-based diffusion charging collision kernel models with canonical experiments. *Journal of Aerosol Science, 140*, 105481. https://doi.org/10.1016/j.jaerosci.2019.105481

Li, L., & Gopalakrishnan, R. (2021). An experimentally validated model of diffusion charging of arbitrary shaped aerosol particles. *Journal of Aerosol Science, 151*, 105678. https://doi.org/10.1016/j.jaerosci.2020.105678

Lin, S. L., & Bardsley, J. N. (1977). Monte Carlo simulation of ion motion in drift tubes. *The Journal of Chemical Physics, 66*(2), 435–445. https://doi.org/10.1063/1.433988

Liu, B., & Goree, J. (2005). Shear viscosity of two-dimensional yukawa systems in the liquid state. *Physical Review Letters, 94*(18), 185002. https://doi.org/10.1103/PhysRevLett.94.185002

Liu, B., & Goree, J. (2007). Superdiffusion in two-dimensional yukawa liquids. *Physical Review E, 75*(1). https://doi.org/10.1103/PhysRevE.75.016405

Liu, B., & Goree, J. (2014). Perpendicular diffusion of a dilute beam of charged dust particles in a strongly coupled dusty plasma. *Physics of Plasmas, 21*(6). https://doi.org/10.1063/1.4885353

Liu, B., & Goree, J. (2016a). Coupling of an acoustic wave to shear motion due to viscous heating. *Physics of Plasmas, 23*(7). https://doi.org/10.1063/1.4956444

Liu, B., & Goree, J. (2016b). Test of the einstein relation in dusty plasmas. *IEEE Transactions on Plasma Science, 44*(4), 483–486. https://doi.org/10.1109/tps.2015.2467966

Liu, B., & Goree, J. (2017). Determination of yield stress of 2d (yukawa) dusty plasma. *Physics of Plasmas, 24*(10). https://doi.org/10.1063/1.4994840

Liu, Z., Suresh, V., & Gopalakrishnan, R. (2020). Effect of volume fraction and hydrodynamic interactions on aerosol particle coagulation using Langevin dynamics simulations. In *Paper presented at the AAAR 38th annual conference*. Virtual Conference.

Liu, P., Ziemann, P. J., Kittelson, D. B., & McMurry, P. H. (1995a). Generating particle beams of controlled dimensions and divergence .1. Experimental evaluation of particle motion in aerodynamic lenses and nozzle expansions. *Aerosol Science and Technology, 22*(3), 293–313. https://doi.org/10.1080/02786829408959748

Liu, P., Ziemann, P. J., Kittelson, D. B., & McMurry, P. H. (1995b). Generating particle beams of controlled dimensions and divergence .2. Experimental evaluation of particle motion in aerodynamic lenses and nozzle expansions. *Aerosol Science and Technology, 22*(3), 314–324. https://doi.org/10.1080/02786829408959749

Lopez-Yglesias, X., & Flagan, R. C. (2013). Ion-aerosol flux coefficients and the steady-state charge distribution of aerosols in a bipolar ion environment. *Aerosol Science and Technology, 47*(6), 688–704. https://doi.org/10.1080/02786826.2013.783684

Loyalka, S. K. (1976). Brownian coagulation of aerosols. *Journal of Colloid and Interface Science, 57*, 578–579.

Lushnikov, A. A., & Kulmala, M. (2004). Flux-matching theory of particle charging. *Physical Review E, 70*(4), Article 046413.

Lushnikov, A. A., & Smirnov, V. I. (1975a). Steady-state coagulation and size distribution of atmospheric aerosols. *Izvestiya Akademii Nauk Sssr Fizika Atmosfery I Okeana, 11*(2), 139–152.

Lushnikov, A. A., & Smirnov, V. I. (1975b). Steady coagulation in distribution of atmospheric aerosol-particles according to size. *Doklady Akademii Nauk SSSR, 222*(5), 1141–1144.

Marlow, W. H. (1980). Derivation of aerosol collision rates for singular attractive contact potentials. *The Journal of Chemical Physics, 73*(12), 6284–6287. https://doi.org/10.1063/1.440126

Masters, A. J., & Madden, P. A. (1981a). A molecular theory of Stokes–einstein behavior. I. Translational brownian motion. *The Journal of Chemical Physics, 74*(4), 2450–2459. https://doi.org/10.1063/1.441368

Masters, A. J., & Madden, P. A. (1981b). A molecular theory of Stokes–einstein behavior. Ii. Rotational diffusion of a brownian sphere. *The Journal of Chemical Physics, 74*(4), 2460–2465. https://doi.org/10.1063/1.441369

Matsoukas, T. (1997). The coagulation rate of charged aerosols in ionized gases. *Journal of Colloid and Interface Science, 187*(2), 474–483. https://doi.org/10.1006/jcis.1996.4723

Matthews, L. S., Land, V., & Hyde, T. W. (2012). Charging and coagulation of dust in protoplanetary plasma environments. *The Astrophysical Journal, 744*(1).

Mazur, P., & Oppenheim, I. (1970). Molecular theory of brownian motion. *Physica, 50*(2), 241–258. https://doi.org/10.1016/0031-8914(70)90005-4

Mazzone, A. M. (2000). Coalescence of metallic clusters: A study by molecular dynamics. *Philosophical Magazine Part A B, 80*(1), 95–111. https://doi.org/10.1080/13642810008218342

McDaniel, W., & Mason, E. A. (1973). *The mobility and diffusion of ions in gases*. Wiley.

Millikan, R. A. (1923). The general law of fall of a small spherical body through a gas, and its bearing upon the nature of molecular reflection from surfaces. *Physical Review, 22*(1), 1–23. https://doi.org/10.1103/PhysRev.22.1

Morán, J., Yon, J., & Poux, A. (2020a). Monte Carlo aggregation code (mcac) part 1: Fundamentals. *Journal of Colloid and Interface Science, 569*, 184–194. https://doi.org/10.1016/j.jcis.2020.02.039

Morán, J., Yon, J., Poux, A., Corbin, F., Ouf, F. X., & Siméon, A. (2020b). Monte Carlo aggregation code (mcac) part 2: Application to soot agglomeration, highlighting the importance of primary particles. *Journal of Colloid and Interface Science, 575*, 274–285. https://doi.org/10.1016/j.jcis.2020.04.085

Naicker, P. K., Cummings, P. T., Zhang, H., & Banfield, J. F. (2005). Characterization of titanium dioxide nanoparticles using molecular dynamics simulations. *The Journal of Physical Chemistry B, 109*(32), 15243–15249. https://doi.org/10.1021/jp050963q

Narsimhan, G., & Ruckenstein, E. (1985a). The brownian coagulation of aerosols over the entire range of knudsen numbers: Connection between the sticking probability and the interaction forces. *Journal of Colloid and Interface Science, 104*, 344–369.

Narsimhan, G., & Ruckenstein, E. (1985b). Monte-carlo simulation of brownian coagulation over the entire range of particle sizes from near molecular to colloidal - connection between collision efficiency and interparticle forces. *Journal of Colloid and Interface Science, 107*(1), 174–193.

Nepal, A., Chiu, G., Xie, J., Singh, G. P., Ploscariu, N., Klankowski, S., Sung, T., Li, J., Flanders, B. N., Hohn, K. L., & Sorensen, C. M. (2015). Highly oxidized graphene nanosheets via the oxidization of detonation carbon. *Applied Physics A-Materials Science & Processing, 120*(2), 543–549. https://doi.org/10.1007/s00339-015-9213-1

Nepal, A., Singh, G. P., Flanders, B. N., & Sorensen, C. M. (2013). One-step synthesis of graphene via catalyst-free gas-phase hydrocarbon detonation. *Nanotechnology, 24*(24), 245602. https://doi.org/10.1088/0957-4484/24/24/245602

Nikbakht, A., Abouali, O., Ahmadi, G., & Asme. (2006). *3-d modelling of brownian motion of nano-particles in aerodynamic lenses*.

Northrup, S. H., Allison, S. A., & McCammon, J. A. (1984). Brownian dynamics simulation of diffusion-influenced bimolecular reactions. *The Journal of Chemical Physics, 80*(4), 1517–1526.

Northrup, S. H., Curvin, M. S., Allison, S. A., & Mccammon, J. A. (1986). Optimization of brownian dynamics methods for diffusion-influenced rate-constant calculations. *The Journal of Chemical Physics, 84*(4), 2196–2203.

Nosenko, V., & Goree, J. (2004). Shear flows and shear viscosity in a two-dimensional yukawa system (dusty plasma). *Physical Review Letters, 93*(15). https://doi.org/10.1103/PhysRevLett.93.155004

Nowakowski, B., & Sitarski, M. (1981). Brownian coagulation of aerosol particles by Monte Carlo simulation. *Journal of Colloid and Interface Science, 83*, 614–622.

Oberreit, D. R., McMurry, P. H., & Hogan, C. J. (2014). Mobility analysis of 2 nm to 11 nm aerosol particles with an aspirating drift tube ion mobility spectrometer. *Aerosol Science and Technology, 48*(1), 108–118. https://doi.org/10.1080/02786826.2013.861893

Ogawa, H. (2005). Molecular dynamics simulation on the single particle impacts in the aerosol deposition process. *Materials Transactions, 46*(6), 1235–1239. https://doi.org/10.2320/matertrans.46.1235

Otto, E., & Fissan, H. (1999). Brownian coagulation of submicron particles. *Advanced Powder Technology, 10*(1), 1–20.

Ouyang, H., Gopalakrishnan, R., & Hogan, C. J. (2012). Nanoparticle collisions in the gas phase in the presence of singular contact potentials. *The Journal of Chemical Physics, 137*(6), Article 064316.

Petrov, O. F., Vaulina, O. S., Fortov, V. E., Molotkov, V. I., Lipaev, A. M., Chernyshev, A. V., Gavrikov, A. V., Shakhova, I. N., Morfill, G. E., Thomas, H., Khrapak, S. A., Semenov, Y. P., Ivanov, A. I., Kaleri, A. Y., Krikalev, S., Zaletin, S. V., & Gidzenko, Y. (2005). Transport of microparticles in weakly ionized gas-discharge plasmas under microgravity. *Microgravity Science and Technology, 16*(1–4), 311–316. https://doi.org/10.1007/bf02945997

Rader, D. J. (1990). Momentum slip correction factor for small particles in nine common gases. *Journal of Aerosol Science, 21*(2), 161–168. https://doi.org/10.1016/0021-8502(90)90001-e

Ratynskaia, S., Regnoli, G., Rypdal, K., Klumov, B., & Morfill, G. (2009). Critical fluctuations and anomalous transport in soft yukawa-Langevin systems. *Physical Review E, 80*(4). https://doi.org/10.1103/PhysRevE.80.046404

Ravi, L., & Girshick, S. L. (2009). Coagulation of nanoparticles in a plasma. *Physical Review E, 79*, Article 026408.

Risken, H., & Frank, T. (1996). *The fokker-planck equation: Methods of solution and applications*. Springer Berlin Heidelberg.

Rohatschek, H., & Zulehner, W. (1987). The resistance force on nonspherical bodies in the free molecule regime. *Journal of Colloid and Interface Science, 119*(2), 378–382. https://doi.org/10.1016/0021-9797(87)90283-9

Rosner, D. E., McGraw, R., & Tandon, P. (2003). Multivariate population balances via moment and Monte Carlo simulation methods: An important sol reaction engineering bivariate example and "mixed" moments for the estimation of deposition, scavenging, and optical properties for populations of nonspherical suspended particles. *Industrial & Engineering Chemistry Research, 42*(12), 2699–2711. https://doi.org/10.1021/Ie020627l

Rotne, J., & Prager, S. (1969). Variational treatment of hydrodynamic interaction in polymers. *The Journal of Chemical Physics, 50*(11), 4831–4837. https://doi.org/10.1063/1.1670977

Sceats, M. G. (1986). Brownian coagulation in a field of force. *The Journal of Chemical Physics, 84*, 5206–5208.

Schuss, Z. (2013). *Brownian dynamics at boundaries and interfaces: In physics, chemistry, and biology*. New York: Springer.

Schweigert, V. A., & Schweigert, I. V. (1996). Coagulation in a low-temperature plasma. *Journal of Physics D: Applied Physics, 29*(3), 655–659. https://doi.org/10.1088/0022-3727/29/3/026

Sharma, G., Wang, Y., Chakrabarty, R., & Biswas, P. (2019). Modeling simultaneous coagulation and charging of nanoparticles at high temperatures using the method of moments. *Journal of Aerosol Science, 132*, 70–82. https://doi.org/10.1016/j.jaerosci.2019.03.011

Shrivastav, V., Nahin, M., Hogan, C. J., & Larriba-Andaluz, C. (2017). Benchmark comparison for a multi-processing ion mobility calculator in the free molecular regime. *Journal of the American Society for Mass Spectrometry, 28*(8), 1540–1551. https://doi.org/10.1007/s13361-017-1661-8

Sitarski, M., & Seinfeld, J. H. (1977). Brownian coagulation in the transition regime. *Journal of Colloid and Interface Science, 61*, 261–271.

Smith, B., Vasut, J., Hyde, T., Matthews, L., Reay, J., Cook, M., & Schmoke, J. (2004). Dusty plasma correlation function experiment. In J. P. Lebreton, C. B. Agee, P. D. Stabekis, P. Bernhardt, & G. I. Ganguli (Eds.), *Scientific exploration, planetary protection, active experiments and dusty plasmas* (Vol. 34, pp. 2379–2383).

Sorensen, C. M., Zhang, H. X., & Taylor, T. W. (1987). Cluster-size evolution in a coagulation-fragmentation system. *Physical Review Letters, 59*(3), 363–366. https://doi.org/10.1103/PhysRevLett.59.363

Soules, J. A. (1990). Precise calculation of the electrostatic force between charged spheres including induction effects. *American Journal of Physics, 58*(12), 1195–1199. https://doi.org/10.1119/1.16251

Sun, X., Lin, T., & Gezelter, J. D. (2008). Langevin dynamics for rigid bodies of arbitrary shape. *The Journal of Chemical Physics, 128*(23), 234107. https://doi.org/10.1063/1.2936991

Suresh, V., Liu, Z., & Gopalakrishnan, R. (2020). Thermodynamic equations of state for the dust grain using Langevin dynamics simulations. In *Paper presented at the AAAR 38th annual conference*.

Tandon, P., & Rosner, D. E. (1999). Monte Carlo simulation of particle aggregation and simultaneous restructuring. *Journal of Colloid and Interface Science, 213*(2), 273–286. https://doi.org/10.1006/jcis.1998.6036

Thajudeen, T., Deshmukh, S., & Hogan, C. J. (2015). Langevin simulation of aggregate formation in the transition regime. *Aerosol Science and Technology, 49*(2), 115–125. https://doi.org/10.1080/02786826.2015.1008971

Thajudeen, T., Gopalakrishnan, R., & Hogan, C. J. (2012). The collision rate of non-spherical particles and aggregates for all diffusive knudsen numbers. *Aerosol Science and Technology, 46*(11).

Thajudeen, T., Hunt, B., & Hogan, C. J. (2014). The single-fiber collision rate and filtration efficiency for nanoparticles ii: Extension to arbitrary-shaped particles. *Aerosol Science and Technology, 48*(8), 886–895. https://doi.org/10.1080/02786826.2014.938799

Thajudeen, T., Jeon, S., & Hogan, C. J. (2015). The mobilities of flame synthesized aggregates/agglomerates in the transition regime. *Journal of Aerosol Science, 80*, 45–57. https://doi.org/10.1016/j.jaerosci.2014.11.003

Trzeciak, T. M., Podgorski, A., & Marijnissen, J. C. M. (2004). Langevin dynamics simulation of aerosol coagulation in highly concentrated systems. [Article]. *Inzynieria Chemiczna i Procesowa, 25*(3), 1741–1746.

Uhlenbeck, G. E., & Ornstein, L. S. (1930). On the theory of the brownian motion. *Physical Review, 36*(5), 823–841. https://doi.org/10.1103/PhysRev.36.823

Vaulina, O. S. (2009). Thermodynamic properties of two-dimensional nonideal structures with isotropic pair potential. *Plasma Physics Reports, 35*(5), 385–393. https://doi.org/10.1134/s1063780x09050031

Vaulina, O. S., & Dranzhevskii, I. E. (2007). Transport properties of quasi-two-dimensional dissipative systems with a screened coulomb potential. *Plasma Physics Reports, 33*(6), 494–502. https://doi.org/10.1134/s1063780x07060062

Vaulina, O. S., & Petrov, O. F. (2004). Simulation of mass transfer in systems with isotropic pair correlation of particles. *Journal of Experimental and Theoretical Physics, 99*(3), 510–521. https://doi.org/10.1134/1.1809679

Vaulina, O. S., Petrov, O. F., & Fortov, V. E. (2004). Analysis of pair correlation functions for macroscopic particles in dusty plasmas: Numerical simulation and experiment. *Journal of Experimental and Theoretical Physics, 98*(3), 515–526. https://doi.org/10.1134/1.1705704

Vaulina, O. S., Petrov, O. F., Gavrikov, A. V., & Fortov, V. E. (2007). Determination of the pairwise interaction potential between dust grains in plasma. *Plasma Physics Reports, 33*(4), 278–288. https://doi.org/10.1134/s1063780x07040034
Vaulina, O. S., Repin, A. Y., & Petrov, O. F. (2006). Empirical approximation for the ion current to the surface of a dust grain in a weakly ionized gas-discharge plasma. *Plasma Physics Reports, 32*(6), 485–488. https://doi.org/10.1134/S1063780X06060055
Vaulina, O. S., Vasilieva, E. V., Petrov, O. F., & Fortov, V. E. (2011). Equilibrium structural properties of two-dimensional nonideal systems. *Epl, 96*(6). https://doi.org/10.1209/0295-5075/96/65003
Veshchunov, M. S., & Azarov, I. B. (2012). Next approximation of the random walk theory for brownian coagulation. *Journal of Aerosol Science, 47*, 70–77. https://doi.org/10.1016/j.jaerosci.2011.12.009
Veshchunov, M. S., & Tarasov, V. I. (2014). Extension of the smoluchowski theory to transitions from dilute to dense regime of brownian coagulation: Triple collisions. *Aerosol Science and Technology, 48*(8), 813–821. https://doi.org/10.1080/02786826.2014.931567
Vincenti, W. G., & Kruger, C. H. (1975). *Introduction to physical gas dynamics*. Huntington, NY: Krieger.
Wagner, P. E., & Kerker, M. (1977). Brownian coagulation of aerosols in rarified gases. *The Journal of Chemical Physics, 66*, 638–646.
Wang, X., Gidwani, A., Girshick, S. L., & McMurry, P. H. (2005). Aerodynamic focusing of nanoparticles: Ii. Numerical simulation of particle motion through aerodynamic lenses. *Aerosol Science and Technology, 39*(7), 624–636. https://doi.org/10.1080/02786820500181950
Wang, X., Kruis, F. E., & McMurry, P. H. (2005). Aerodynamic focusing of nanoparticles: I. Guidelines for designing aerodynamic lenses for nanoparticles. *Aerosol Science and Technology, 39*(7), 611–623. https://doi.org/10.1080/02786820500181901
Wu, X., & Brooks, B. R. (2011). Toward canonical ensemble distribution from self-guided Langevin dynamics simulation. *The Journal of Chemical Physics, 134*(13), 134108. https://doi.org/10.1063/1.3574397
Yamakawa, H. (1970). Transport properties of polymer chains in dilute solution: Hydrodynamic interaction. *The Journal of Chemical Physics, 53*(1), 436–443. https://doi.org/10.1063/1.1673799
Yi, M.-Y., Kim, D.-S., Lee, J.-W., & Koplik, J. (2005). Molecular dynamics (md) simulation on the collision of a nano-sized particle onto another nano-sized particle adhered on a flat substrate. *Journal of Aerosol Science, 36*(12), 1427–1443. https://doi.org/10.1016/j.jaerosci.2005.03.013
Zahaf, R., Kim, S.-K., Shin, J., Park, K., Choi, T.-Y., & Lee, D. (2015). Effect of volume fraction on transient structural behavior of aerosol particles using off-lattice kinetic Monte Carlo simulation. *Aerosol Science and Technology, 49*(12), 1242–1255. https://doi.org/10.1080/02786826.2015.1116681
Zhang, C., Thajudeen, T., Larriba, C., Schwartzentruber, T. E., & Hogan, C. J. (2012). Determination of the scalar friction factor for nonspherical particles and aggregates across the entire knudsen number range by direct simulation Monte Carlo (dsmc). *Aerosol Science and Technology, 46*(10), 1065–1078. https://doi.org/10.1080/02786826.2012.690543. doi: 10.1080/02786826.2012.690543.
Zhou, H. X., Szabo, A., Douglas, J. F., & Hubbard, J. B. (1994). A brownian dynamics algorithm for calculating the hydrodynamic friction and the electrostatic capacitance of an arbitrarily-shaped object. *The Journal of Chemical Physics, 100*(5), 3821–3826.
Zhu, H. (1996). Sintering processes of two nanoparticles: A study by molecular dynamics simulations. *Philosophical Magazine Letters, 73*(1), 27–33. https://doi.org/10.1080/095008396181073

Vikram Suresh is currently a PhD candidate in the Department of Mechanical Engineering at The University of Memphis. His doctoral research is focused on modeling particle-level and particle-phase level processes in plasmas using Langevin Dynamics methods and trajectory analysis. He received his Master of Science degree in Mechanical Engineering from the Arizona State University and Bachelor of Technology degree in Mechanical Engineering from S.R.M. University, Chennai, India. His research interests include dusty-plasmas, particle trajectory analysis, and thin-film/coating technologies.

Ranganathan Gopalakrishnan is currently the UMRF Ventures Assistant Professor of Mechanical Engineering at The University of Memphis since 2016. He obtained his PhD in Mechanical Engineering from the University of Minnesota in 2013 and Bachelor of Technology degree in Mechanical Engineering from the National Institute of Technology, Tiruchirappalli, India in 2008. His research interests include particulate transport processes in aerosols, dusty plasmas, and ionized gases. He is a recipient of the DOE EARLY CAREER award for the year FY2020 from the Office of Fusion Energy Sciences, US Department of Energy Office of Science (SC).